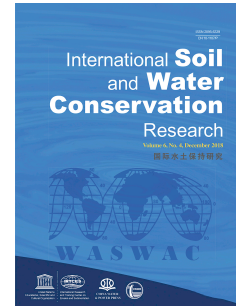


Journal Pre-proof

Gully erosion mapping susceptibility in a Mediterranean environment: A hybrid decision-making model

Sliman Hitouri, Mohajane Meriame, Ali Sk Ajim, Quevedo Renata Pacheco, Thong Nguyen-Huy, Pham Quoc Bao, Ismail ElKhrachy, Antonietta Varasano



PII: S2095-6339(23)00089-8

DOI: <https://doi.org/10.1016/j.iswcr.2023.09.008>

Reference: ISWCR 449

To appear in: *International Soil and Water Conservation Research*

Received Date: 1 March 2023

Revised Date: 25 September 2023

Accepted Date: 26 September 2023

Please cite this article as: Hitouri S., Meriame M., Sk Ajim A., Renata Pacheco Q., Nguyen-Huy T., Quoc Bao P., ElKhrachy I. & Varasano A., Gully erosion mapping susceptibility in a Mediterranean environment: A hybrid decision-making model, *International Soil and Water Conservation Research* (2023), doi: <https://doi.org/10.1016/j.iswcr.2023.09.008>.

This is a PDF file of an article that has undergone enhancements after acceptance, such as the addition of a cover page and metadata, and formatting for readability, but it is not yet the definitive version of record. This version will undergo additional copyediting, typesetting and review before it is published in its final form, but we are providing this version to give early visibility of the article. Please note that, during the production process, errors may be discovered which could affect the content, and all legal disclaimers that apply to the journal pertain.

© 2023 International Research and Training Center on Erosion and Sedimentation, China Water and Power Press, and China Institute of Water Resources and Hydropower Research. Publishing services by Elsevier B.V. on behalf of KeAi Communications Co. Ltd.

**Gully erosion mapping susceptibility in a Mediterranean environment: a hybrid
decision-making model**

Sliman Hitouri¹, Mohajane Meriame^{2,*}, Sk Ajim Ali³, Renata Pacheco Quevedo⁴, Thong
Nguyen-Huy⁵, Quoc Bao Pham⁶, Ismail ElKhrachy⁷, and Antonietta Varasano⁸

¹Geosciences Laboratory, Department of Geology, Faculty of Sciences, University Ibn Tofail,
Kenitra 14000, Morocco

²Construction Technologies Institute, National Research Council of Italy, Polo Tecnologico di
San Giovanni a Teduccio, 80146 Napoli, Italy

³Department of Geography, Faculty of Science, Aligarh Muslim University (AMU), Aligarh,
UP 202002, India

⁴Earth Observation and Geoinformatics Division, National Institute for Space Research
(INPE), Sao Jose dos Campos, Sao Paulo, 12227010, Brazil

⁵Centre for Applied Climate Sciences, University of Southern Queensland, Toowoomba, 4350,
QLD, Australia

⁶Faculty of Natural Sciences, Institute of Earth Sciences, University of Silesia in Katowice,
Będzińska street 60, 41-200, Sosnowiec, Poland

⁷College of Engineering, Civil Engineering Department, Najran University, Najran 66291,
Saudi Arabia

⁸ITC-CNR, Construction Technologies Institute, National Research Council, 70124 Bari, Italy

*Correspondence: mohajane@itc.cnr.it

Gully erosion mapping susceptibility in a Mediterranean environment: a hybrid decision-making model

Abstract

Gully erosion is one of the main natural hazards, especially in arid and semi-arid regions, destroying ecosystem service and human well-being. Thus, gully erosion susceptibility maps (GESM) are urgently needed for identifying priority areas on which appropriate measurements should be considered. Here, we proposed four new hybrid Machine learning models, namely weight of evidence -Multilayer Perceptron (MLP- WoE), weight of evidence –K Nearest neighbors (KNN- WoE), weight of evidence - Logistic regression (LR- WoE), and weight of evidence - Random Forest (RF- WoE), for mapping gully erosion exploring the opportunities of GIS tools and Remote sensing techniques in the El Ouair watershed located in the Souss plain in Morocco. Inputs of the developed models are composed of the dependent (i.e., gully erosion points) and a set of independent variables. In this study, a total of 314 gully erosion points were randomly split into 70% for the training stage (220 gullies) and 30 % for the validation stage (94 gullies) sets were identified in the study area. 12 conditioning variables including elevation, slope, plane curvature, rainfall, distance to road, distance to stream, distance to fault, TWI, lithology, NDVI, and LU/LC were used based on their importance for gully erosion susceptibility mapping. We evaluate the performance of the above models based on the following statistical metrics: Accuracy, precision, and Area under curve (AUC) values of receiver operating characteristics (ROC). The results indicate the RF- WoE model showed good accuracy with (AUC = 0.8), followed by KNN- WoE (AUC = 0.796), then MLP-WoE (AUC = 0.729) and LR-WoE (AUC = 0.655), respectively. Gully erosion susceptibility maps provide information and valuable tool for decision-makers and planners to identify areas where urgent and appropriate interventions should be applied.

25 **1. Introduction**

26 Understanding how to use natural resources is essential to the existence of human communities.
27 In addition to supporting basic human requirements like food, clean water, and air, soils are an
28 important transporter for biodiversity. The depletion of natural resources, particularly soil, is one
29 of the major issues of the modern era that has emerged in the past ten years (Turner et al., 2016;
30 Wassie, 2020). Soil degradation is caused by population increase and resource extraction, which
31 endangers human lives and property (Gomiero, 2016; Scherr, 2000). Soil erosion may impact soil
32 productivity, surface water sources, their quality, ecological balance, and landscape (Bilotta et al.,
33 2007; Issaka and Ashraf, 2017). Preventing land degradation proves to be challenging. Among the
34 various types of soil erosion, gully erosion stands out as one of the most complex and hazardous
35 forms, given its capacity to displace substantial amounts of soil. A gully is characterized as a deep,
36 relatively permanent canal with vertical walls on either side that allow passing water currents for
37 a short period. Gully erosion occurs when rushing surface water erodes a deep channel, removing
38 and transporting the eroded surface soil (Ghorbanzadeh et al., 2020a). Over time, these gullies
39 cause soil erosion, alter the surrounding environment, and accelerate the sedimentation of rivers
40 and dams (Belayneh et al., 2020; Ghorbanzadeh et al., 2020a; Hancock and Evans, 2010). One of
41 the most important techniques for managing this phenomenon is understanding the variables
42 influencing the incidence of this form of erosion and its zoning. Gully erosion affects the
43 environment in two ways: first, by eroding the surface and diminishing and reducing soil horizons,
44 leading to high sediment production and bedding degradation; and second, by escalating surface
45 discharge and decreasing groundwater nutrition.

46 In Morocco, gully erosion is one of the most significant environmental problems increasingly
47 posing a threat to the country (Azedou et al., 2021; d'Oleire-Oltmanns et al., 2014; Meliho et al.,

48 2018). There are several different types of soil erosion impacting half of Morocco's 20 million-
49 hectare watersheds, such as sheet, rill, splash, and gully, which result in around 100 million tonnes
50 of soil annually (Mosaid et al., 2022; Tairi et al., 2021). The gully is the most harmful type of
51 erosion, causing several times more damage than other types of erosion, such as sedimentation of
52 dams, destruction of energy and transportation transmission lines, loss of farmland productivity,
53 land degradation, and long-term adverse economic effects (Belasri and Lakhouili, 2016;
54 Bouslihim, 2020; Meliho et al., 2018). Even though there are anthropogenic causes for the
55 generation of gullies, it is sped up by variables including climate change, geologic conditions, and
56 soil characteristics (Nir et al., 2021; Poesen et al., 2003). In this sense, the framework of watershed
57 management includes mapping and monitoring of regions susceptible to gully erosion.

58 Many conventional and numerical techniques were used for gully susceptibility mapping, by
59 linking gully occurrence and conditioning factors (Jaafari et al., 2022; Rahmati et al., 2017). Field
60 survey and data collection, although effective in mapping and evaluating gully erosion, are
61 characterized by their time-consuming and labour-intensive nature, besides cannot forecast the
62 spatial development of gully erosion (Jiang et al., 2021). As an alternative, the Water Erosion
63 Prediction Project (Ghorbanzadeh et al., 2020b) and the European Soil Erosion Model (Quarteroni
64 and Veneziani, 2003) applied physically-built models to estimate gully erosion. These models are
65 less suitable for regional-scale study since they need extensive data and labor-intensive calibration
66 procedures (Momm et al., 2012; Yuan et al., 2020). In addition, these models are adequate for
67 numerically estimating the amount of gully erosion, however, they are less appropriate for gully
68 erosion susceptibility mapping (Garosi et al., 2018; Rahmati et al., 2016).

69 The generation of gully erosion susceptibility maps currently uses a variety of probabilistic,
70 knowledge-driven, and machine learning methods, including bivariate statistics (Melihho et al.,

71 2018), weights-of-evidence (Shit et al., 2020), logistic regression (Conoscenti et al., 2014),
72 information value (Paul and Saha, 2019), random forest (Avand et al., 2019), bivariate statistical
73 models (Lana et al., 2022), maximum entropy (Azareh et al., 2019), frequency ratio (Amare et al.,
74 2021), artificial neural network (Gafurov and Yermolayev, 2020), Functional tree (Tien Bui et al.,
75 2019), Naïve Bayes tree (Hosseinalizadeh et al., 2019), support vector machine (Karami et al.,
76 2015), and boosted regression trees (Arabameri et al., 2019).

77 When there is insufficient data about the intensity and distribution of a phenomenon, such as gully
78 erosion, GIS-based multi-criteria decision analysis (MCDA) models can be useful. The analytical
79 hierarchy process (AHP) and analytical network process (ANP), two qualitative (knowledge-
80 based) MCDA, have been applied to gully susceptibility mapping in various study areas
81 (Arabameri et al., 2019, 2018a; Chakraborty and Pal, 2023; Choubin et al., 2019; Nhu et al., 2020).
82 Although these models appear to offer solutions for environmental susceptibility mapping, their
83 major limitation is the uncertainty associated with the experts' assessments, which can occasionally
84 result in inaccurate conclusions (Ghorbanzadeh et al., 2020b).

85 Machine Learning is a cutting-edge method for anticipating gully erosion as well as managing and
86 minimising the harm this phenomenon causes (Chakraborty and Pal, 2023). The use of Machine
87 Learning algorithms in studies of natural hazards, such as floods, wildfires, sinkholes, droughts,
88 earthquakes, land subsidence, groundwater, landslides, and gullies, has significantly advanced
89 (Abu El-Magd et al., 2021; Ali et al., 2022, 2021, 2020; Ghorbanzadeh et al., 2019; Hitouri et al.,
90 2022; Pham et al., 2021). There are some advantages of using machine learning algorithms for
91 gully susceptibility mapping, such as being non-parametric. Researchers have applied tree-based
92 machine learning techniques for gully erosion modelling, which outperformed traditional
93 techniques in terms of performance and accuracy (Mohsin et al., 2022). The overfitting issue in

94 these tree-based algorithms is quite minimal when compared to numerical models (Ajit, 2016).
95 Moreover, backpropagation is a supervised learning method that is used by MLP during training.
96 MLP differs from a linear perceptron due to its numerous layers and non-linear activation (Pham
97 et al., 2022). One or more secret layers can be found in an MLP (apart from one input and one
98 output layer). A multi-layer perceptron can learn non-linear functions in addition to linear
99 functions, whereas a single-layer perceptron can only learn linear functions (Parvin et al., 2022).
100 LR is more straightforward to use, comprehend, and train than other methods (Davis et al., 2016).
101 Fitting the line values to the sigmoid curve is the goal of LR (Yin et al., 2020). The KNN method
102 has the benefits of being flexible to different proximity calculations, being relatively intuitive, and
103 using a memory-based approach (Merghadi et al., 2020).

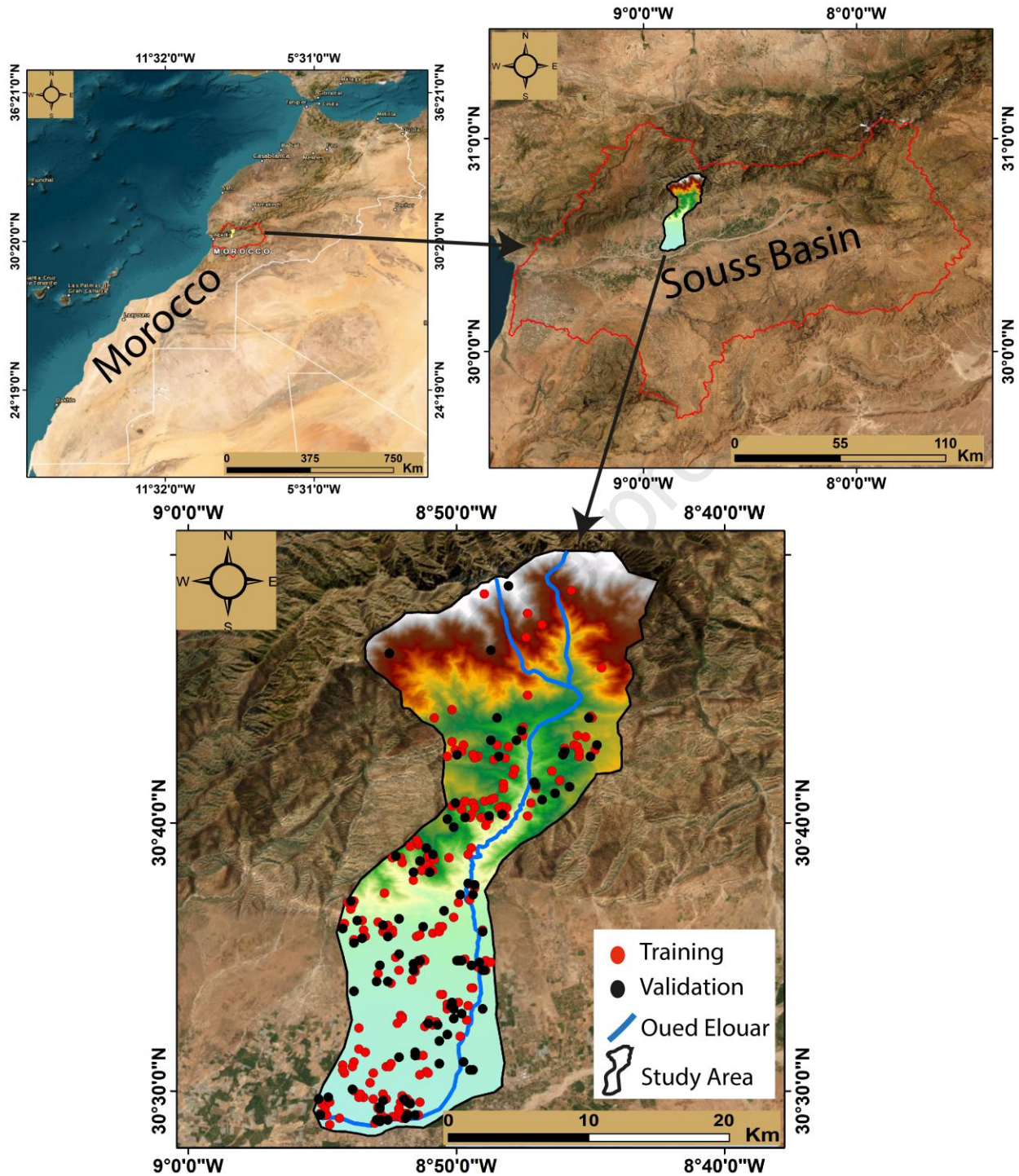
104 In this sense, the main aim of this study was to present four new hybrid Machine Learning
105 models for mapping gully erosion in the province of Taroudant, located in the Souss plain of
106 Morocco, namely: i) weight of evidence - Multilayer Perceptron (MLP- WoE); ii) weight of
107 evidence -K Nearest neighbors (KNN- WoE); iii) weight of evidence - Logistic regression (LR-
108 WoE); iv) weight of evidence - Random Forest (RF- WoE). These ensemble models are a novel
109 method that has not been used for gully erosion susceptibility in this area before. The RF, MLP,
110 LR, and KNN algorithms were considered taking into account their advantages. In addition , the
111 study integrated the WOE with the four machine learning algorithms due to its powerful ability to
112 transform and select variables, and reveals the predictive ability of an independent variable in
113 relation to the dependent variable (Elmoulat and Ait Brahim, 2018; Shafizadeh-Moghadam et al.,
114 2017). For that, we followed these steps, (1) using multi-collinearity analysis to identify significant
115 gully erosion conditioning factors, (2) creating the hybrid machine learning models to predict gully
116 erosion susceptibility, (3) employing the k-fold cross-validation (CV) method to mitigate the

117 negative effects of randomness on the results, and (4) assessing the capability and robustness of
118 the four hybrid models by comparing their performance using the Receiver Operating
119 characteristic Curve (ROC).

120 While there have been many recent advances and applications of Machine Learning techniques for
121 gully erosion mapping studies in various study areas worldwide, their applicability in regions with
122 limited ground-based data or inadequate data quality remains uncertain. To fill this gap, our study
123 contributes to the literature by emphasizing the importance of using freely available data sources
124 to identify and map gully erosion susceptibility in this watershed.

125 **2. Study area**

126 El Ouaar watershed is located in the province of Taroudant, Morocco. It is limited between
127 longitudes ($8^{\circ}43'30''$ W - $8^{\circ}56'30''$ W), and latitudes ($30^{\circ}28'00''$ N - $30^{\circ}50' 00''$ N). El Ouaar
128 watershed covers an area of 395.18 km^2 and is characterized by an arid and semi-arid climate.
129 From a topographical point of view, the study area shows an altitude ranging between 214, located
130 in the south of the basin, and an altitude of 3353 m, located in the north, with an average elevation
131 of 1657.5 m and an average slope of 19° (Fig.1).The annual rainfall in the area varies significantly,
132 ranging from 207 mm to 625 mm during the winter season, while temperatures tend to be cooler,
133 averaging around 6.4°C . In August, temperatures sometimes reach 45°C (Dijon, 1966).



134

135

Fig. 1 Location of the study area.

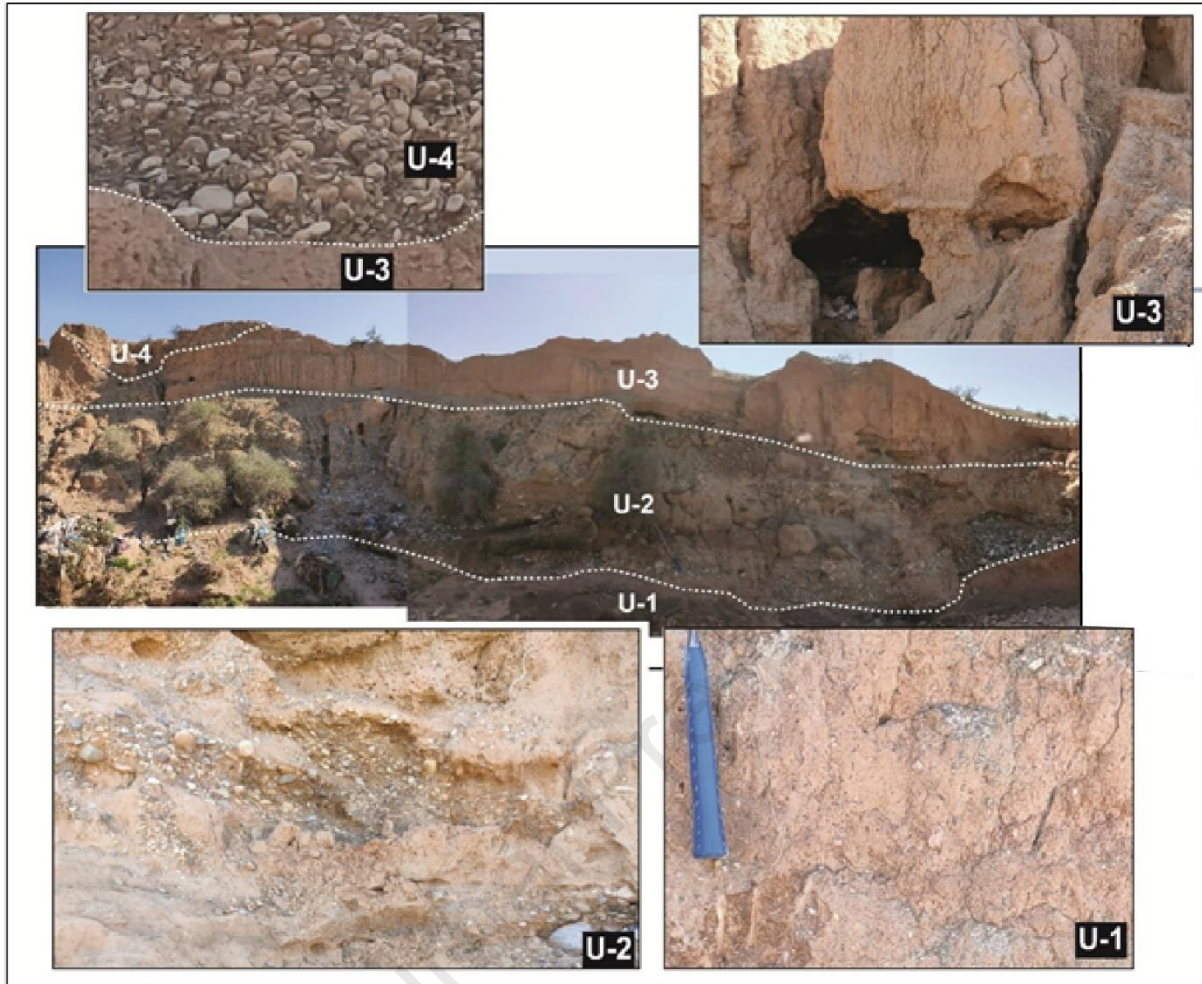
136 Geologically, El Ouwar watershed is characterized by a silty and clay lithological terrain of

137 Quaternary age. The north part of this study area is presented by the Cretaceous basement

138 containing carbonate lithology dominated by dolomite and limestone. The study area is a part of
139 the Souss basin, which is limited to the north by the High Atlas ranges and to the south by the
140 Anti-Atlasic ranges. It is characterized by quaternary lithological units, in the north of this basin
141 where the limestone and dolomite deposits of Cretaceous are very dominant and the schistose
142 Paleozoic deposits. In the center of this basin at the level of the plain of Souss there are only the
143 quaternary deposits not very compact, especially the silts and the clays. The quaternary formations
144 are constituted by four lithostratigraphic units (Figs. 2 and 3).

- 145 - The first 2 m of a basal unit (U1), whitish, massive, consisting of silt-sandstone
146 encrusted and more consolidated than the overlying deposits. U1 is most likely thicker
147 at depth;
- 148 - 2 m of a sandy-limono-conglomeratic unit (U2), made up of grano-decreasing
149 sequences where the conglomerates are polygenic lenticular, with a more or less friable
150 sandy matrix. 2.5 m of a unit (U3) made up of red-brown sandy-clayey silts with small
151 pebbles and rare microconglomeratic pockets.
- 152 - 0.5 to 1 m of an alluvial unit (U4) consisting of polygenic conglomerate with a silty-
153 sandy matrix. The elements are well blunted and rounded, where their size varies from
154 a few millimeters to a few centimeters and are of varied nature: limestone, sandstone,
155 and magmatic rocks. The north of the El Ouair watershed, the Western High Atlas is
156 characterized by a Paleozoic terrain rich in sandstone and shale, and the Cretaceous,
157 contains carbonate rocks especially limestone and dolomite (Ambroggi, 1963).

158



159

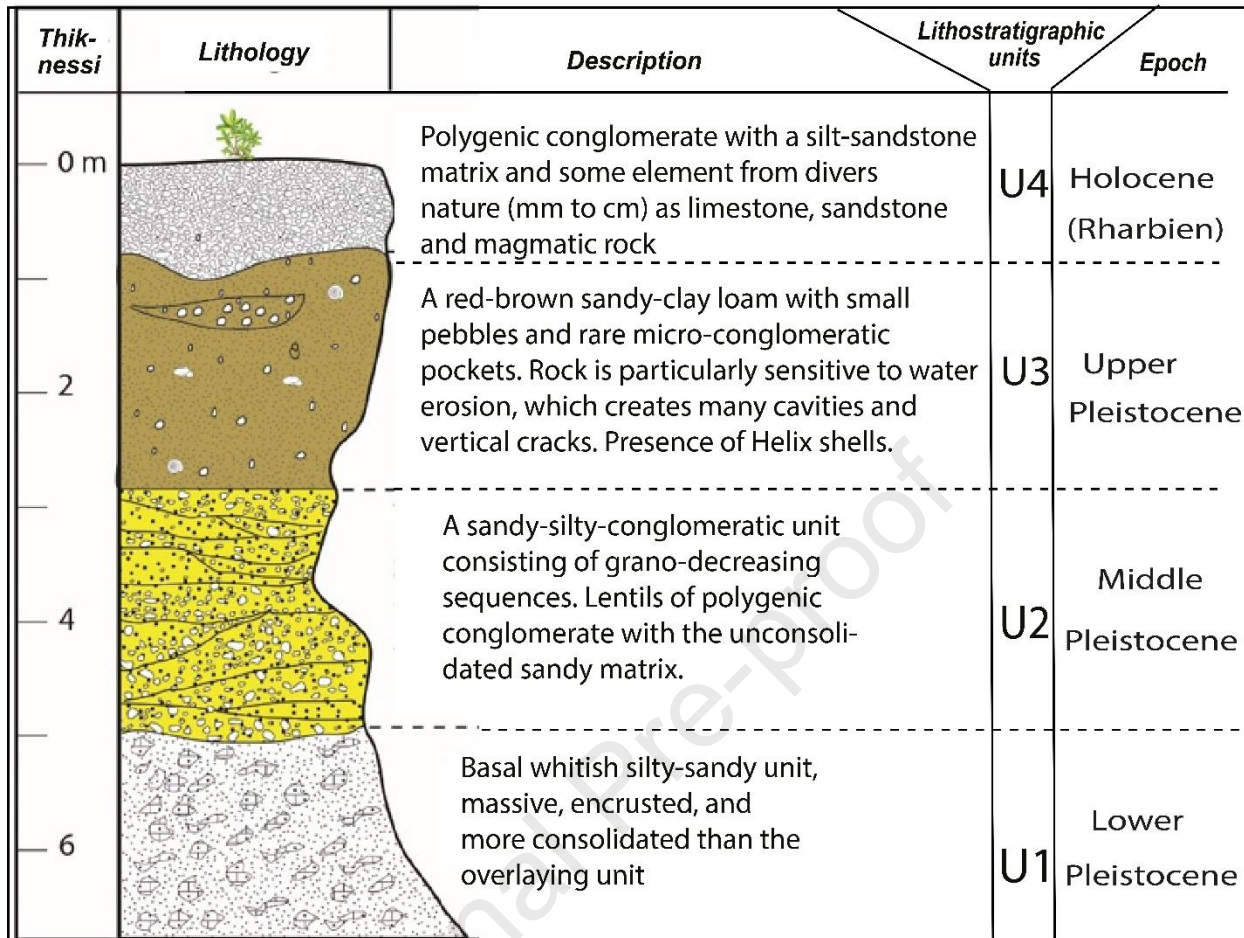
160

161

162

163

Fig. 2 : Quaternary lithostratigraphic deposits in the study area.



164

165

Fig. 3: Quaternary lithostratigraphic deposits in the study area.

166

3. Data and Methodology

167

The procedure followed in this is divided into three main parts: data collection and processing, ML

168

implementation, and model performance assessment. All ML models elaborated in this study were

169

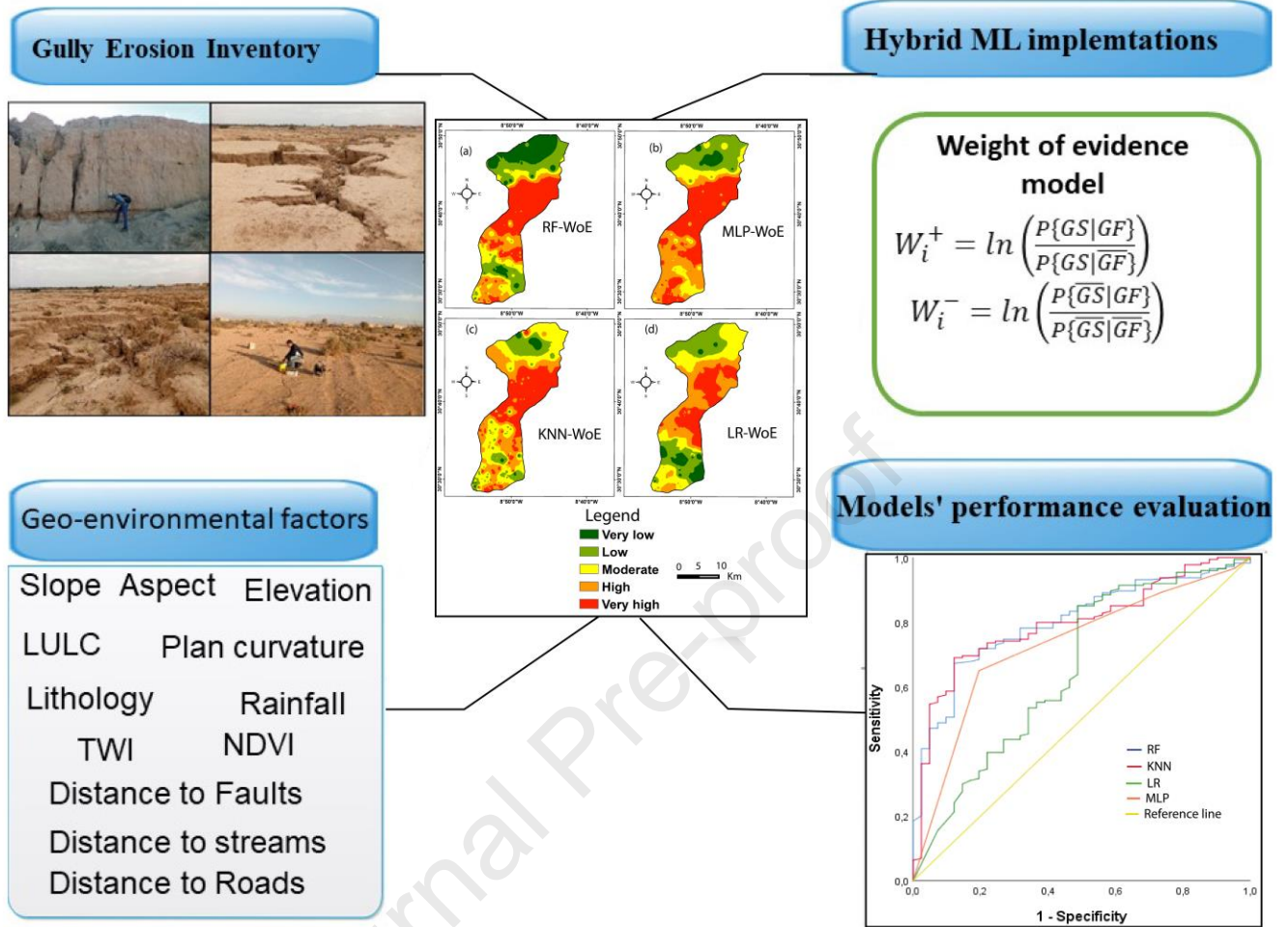
developed in an R programming environment and GESM was reclassified into five classes: “very

170

low”, “low”, “moderate”, “high” and “very high” susceptibility, using the natural breaks method

171

in ArcGIS software. The methodology of the present work is presented in Fig. 4.



172

173

Fig. 4: The methodology adopted in this study.

174 3.1. Inventory of gully erosion locations

175 Gully erosion inventory is a primary and crucial step of gully erosion mapping. In this study, gully
 176 erosion points were collected from a variety of sources including field data and high-resolution
 177 aerial images in Google Earth. During the field survey, gully points were collected with their
 178 geographical coordinates using Global Positioning System (GPS) tools. The gully points in the
 179 study area showed that the width of erosion can reach 4 m, with a depth varying from 0.5 to 2m,
 180 and sometimes can reach 3m, especially in areas near the Wadi El Ouaar. Infrastructures and
 181 natural resources (e.g., roads, schools, and agricultures areas) are strongly influenced by water
 182 erosion in this region (Fig. 5). Gully erosion points were randomly divided into training and

183 validation datasets in the ratio of 70 % (220 points) and 30 % (94 points) for models
184 implementations. Also, a total of 314 non-gully erosion points were collected and randomly
185 divided into 70% (220 points) and 30% (94 points) for training and testing, respectively. The gully
186 erosion locations were assigned the value “1” and the non-gully erosion locations were assigned
187 the value “0”.

188



189

190

Fig. 5: Gully erosion in El Ouaar watershed from a field survey.

191

192

193

194 **3.2. Gully erosion conditioning factors**

195 Determination of environmental factors is the first step in gully erosion susceptibility modelling
 196 for identifying important factors that contribute to gully occurrence in a given terrain (Rahmati et
 197 al., 2017). In this study, 12 geo-environmental factors were selected, these include: Elevation, Plan
 198 curvature, Aspect, Slope, Rainfall, Lithology, Land use/land cover, NDVI, Distance to roads,
 199 Distance to streams, Distance to faults, Topographic Wetness Index (TWI) (See Table 1 for
 200 details).

201 **Table 1** Details of thematic data layers and data sources used in this study

Data	Data types in GIS	Scale	Source
Erosion inventory	Polygon	–	Google earth and field data
Elevation	Grid	30×30 m	DEM 30 m, from https://earthexplorer.usgs.gov/ (accessed on 20 August 2021)
Aspect	Grid	30×30 m	DEM 30 m, from https://earthexplorer.usgs.gov/ (accessed on 20 August 2021)
Slope	Grid	30×30 m	DEM 30 m, from https://earthexplorer.usgs.gov/ (accessed on 20 August 2021)
Plan curvature	Grid	30×30 m	DEM 30 m, from https://earthexplorer.usgs.gov/ (accessed on 20 August 2021)
TWI	Grid	30×30 m	DEM 30 m, from https://earthexplorer.usgs.gov/ (accessed on 20 August 2021)
Rainfall	Grid	30×30 m	ERA-Interim, from https://apps.ecmwf.int/datasets/ (accessed on 18 July 2021)
NDVI	Grid	30×30 m	Landsat-8-OLI image, from https://earthexplorer.usgs.gov/ (accessed on 12 July 2021)
Lithology	Polygon	-	Geological map of Morocco at a scale of 1:000 000
Faults	Polygon	-	Geological map of Morocco at a scale of 1:000 000
Roads	Polygon	-	https://www.geojamal.com
Streams	Polygon	-	https://geossc.ma
Land use land cover	Polygon	-	Landsat-8-OLI image, from https://earthexplorer.usgs.gov/

3.2.1. Elevation

Elevation is an important factor in the evolution of susceptibility to gully erosion, based on the occurrence and development of the gully erosion (Zabihi et al., 2018), because it affects vegetation, precipitation, and gully erosion (Golestani et al., 2014). This factor was reclassified into three classes: 1801-3353 m; 792-1801 m and 214 -792 m (Fig.6a).

3.2.2. Slope angle

Slope runoff and surface drainage contribute to erosion (Ghorbani Nejad et al., 2017). It is considered to be an important predictor of gully erosion processes (Conforti et al., 2011; Lucà et al., 2011). This factor was reclassified into five classes: 0-7.23%, 7.23-15.75%, 15.75-24.79%, 24.79 -35.13% and 35.13-65.86% (Fig. 6b).

3.2.3. Aspect

Aspect is an important conditioning factor in gully erosion mapping, it determines the direction of the slope in the basin. In this study, this factor is extracted from the DEM of Morocco. It is defined by the following equation (Zhou and Liu, 2004).

$$Aspect = 270^\circ + \arctan\left\{\frac{\mathcal{F}_y}{\mathcal{F}_x}\right\} - 90^\circ \frac{\mathcal{F}_x}{\mathcal{F}_y} \quad (1)$$

$$\mathcal{F}_x = \frac{Z_8 - Z_2}{2\omega} \quad (2)$$

$$\mathcal{F}_y = \frac{Z_6 - Z_4}{2\omega} \quad (3)$$

Where Z_1 to Z_9 are cells of the 30×30 moving window and W is the grid resolution. The aspect factor map shows nine classes: Flat (F), North (N), Northeast (NE), East (E), South (S), Southwest (SW), West (W), and Northwest (NW) (Fig. 6c).

224 **3.2.4. Plan curvature**

225 Plan curvature contributes to the divergence or convergence of the water distribution and is
226 generally defined as the curvature of the contour line that is formed by the intersection of a
227 horizontal plan and the surface (Hitouri et al., 2022; Rahmati et al., 2022). The negative value
228 represents the concave area, the positive value refers to the convex area and the zero value indicates
229 the flat area (Fig. 6d).

230 **3.2.5. Distance to road**

231 Roads facilitate transportation and removal of eroded upland matter (Conoscenti et al., 2014).
232 The road distance map was extracted from the road network map of Morocco, using the
233 Euclidean distance tool available in ArcGIS software (version 10.8). It was subdivided into five
234 classes: 1 – 1,308m; 1,308- 2,956m; 2,956- 4,894m; 4,894 -7,462 and 7,462 -12,357 m (Fig. 7a).

235 **3.2.6. Distance to stream**

236 This factor allows us to study the influence of the watercourses on gully erosion. It has an impact
237 on erosion activities and also influences the wetting capacity of the surface. The values of this
238 factor are classified into five categories: 0–1,229m; 1,229–2,683m; 2,683–4,322m; 4,322–6,297m
239 and 6,297–9,502m (Fig. 7b).

240 **3.2.7. Distance to faults**

241 This factor is based on the geological structure of the study area. It was extracted from the
242 geological map of Morocco with a scale of 1,000,000 and from the faults detected during the
243 mission fields and from the interpretation of geophysical data. It is characterized by values
244 classified into five categories: 0–2,184 m; 2,184–4,817m; 4,817–7,561m; 7,561–10,586m and
245 10,586–14,283m (Fig. 7c).

246

247 **3.2.8. Rainfall**

248 Rainfall determines the probability of gully occurrence in a given area. It represents the climate
 249 conditions of a study area (Roy and Saha, 2019). The annual average rainfall of the study area is
 250 416 mm. We used the Inverse Distance-Weighted (IDW) interpolation method for preparing the
 251 rainfall map of El Ouair watershed. Rainfall data used in this study were downloaded from
 252 (<https://apps.ecmwf.int/datasets>, accessed on 18 July 2021) and classified into five classes: 207–
 253 273 mm, 273–363 mm, 363–443 mm, 443–525 mm, and 525–625 mm (Fig. 7d).

254 **3.2.9. TWI**

255 The topographic wetness index calculates the quantity of water in the study area, which contributes
 256 to gully erosion (Moore and Wilson, 1992). It is defined by applying the following equation
 257 (Moore et al., 1991):

$$258 \quad TWI = \ln(A_s / \tan\beta) \quad (4)$$

259 Where A_s is the basin area and β is the slope gradient in degrees.

260 In this study, TWI was classified into five classes: -6.50 – (-5.53); -5.53 – -1.55; 1.55 – 4.76, and
 261 4.76 – 12.51 (Fig. 8a).

262 **3.2.10. Lithology**

263 The lithology plays an important role in erosion; it is considered a fundamental variable for
 264 mapping the susceptibility of dust sources and terrain. It allows us determining the source areas
 265 with low hardness compared to other resistant units as well as the nature and types of soil
 266 (Sissakian et al., 2013). The lithology layer of this area study was prepared by digitizing the
 267 geological map of Morocco at a 1:1000,000 scale, and field data.

268 The study area is composed of nine geological formations: A) Upper Pleistocene and Holocene,
 269 B) Middle and Upper Miocene, C) Phosphate Eocene, D) High Cretaceous, E) Upper Cretaceous

270 phosphate facies, F) Middle Cretaceous, G) Granites and granodiorites (Tichka and Jbilet), H)
271 Ordovician, I) Cambrien (Fig. 8b).

272 **3.2.11. Land use / Land cover**

273 This factor controls the occurrence of gullies, depending on the type of land use/ Land cover (Band
274 et al., 2020). It indicates a negative correlation between erosion rate and vegetation density
275 (Hughes et al., 2001). In this study, one Landsat 8 Operational Land Imager (OLI) satellite image
276 acquired on 12 July 2021, downloaded from the United States Geological Survey website (USGS)
277 was used for land cover / land use information. Therefore, the radiometric and atmospheric
278 corrections are performed based on the Dark Object Subtraction (DOS) algorithm in ENVI 5.2
279 software. After, the land cover classification process was applied using Support Vector Machine
280 (SVM) supervised classifier and five land cover / land use (LULC) classes were identified, namely,
281 water, greenhouses, barelands, construction/buildings, and agricultural land (Fig. 8c).

282 A total of 150 training sample points, i.e., 30 samples per LULC class, were done by visual and
283 manual on-screen digitizing based on our expert knowledge of the study area and high-resolution
284 imagery from Google Earth. The generated land cover output achieved an overall accuracy of
285 95.32%.

286 **3.2.12. NDVI**

287 The Normalized Difference Vegetation Index (NDVI) represents a good indicator of
288 photosynthetic activity (Pourghasemi et al., 2014). In our study, NDVI was calculated using one
289 Landsat 8 OLI satellite image acquired on 12 July 2021 downloaded from the United States
290 Geological Survey website (USGS) website following equation 5. NDVI was calculated and
291 reclassified into 5 classes using ArcGIS 10.8.

$$292 \quad \text{NDVI} = \frac{\text{NIR}-\text{Red}}{\text{NIR}+\text{Red}} \quad (5)$$

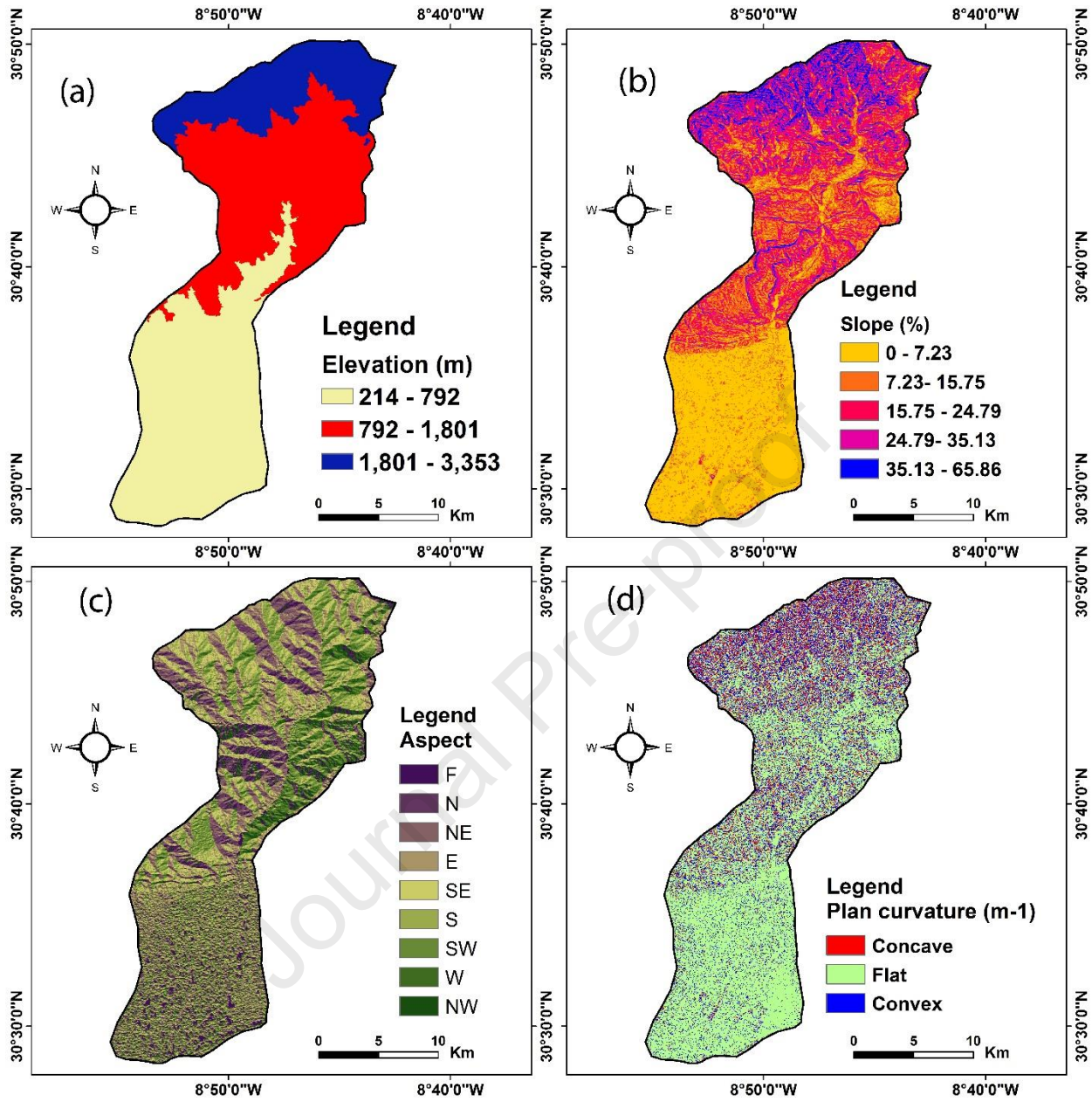
293 Where NIR and Red values represent the infrared and red portion of the electromagnetic spectrum
294 respectively. For Landsat 8 OLI image, the NIR and RED bands are band 5 (0.85–0.88 μm) and
295 band 4 (0.64–0.67 μm), respectively. After, NDVI values were reclassified into 5 classes: (-0.30-
296 0.12), (0.12-0.17), (0.17-0.25), (0.25-0.36), and (0.36-0.71) (Fig. 8d).

297

298

299

Journal Pre-proof

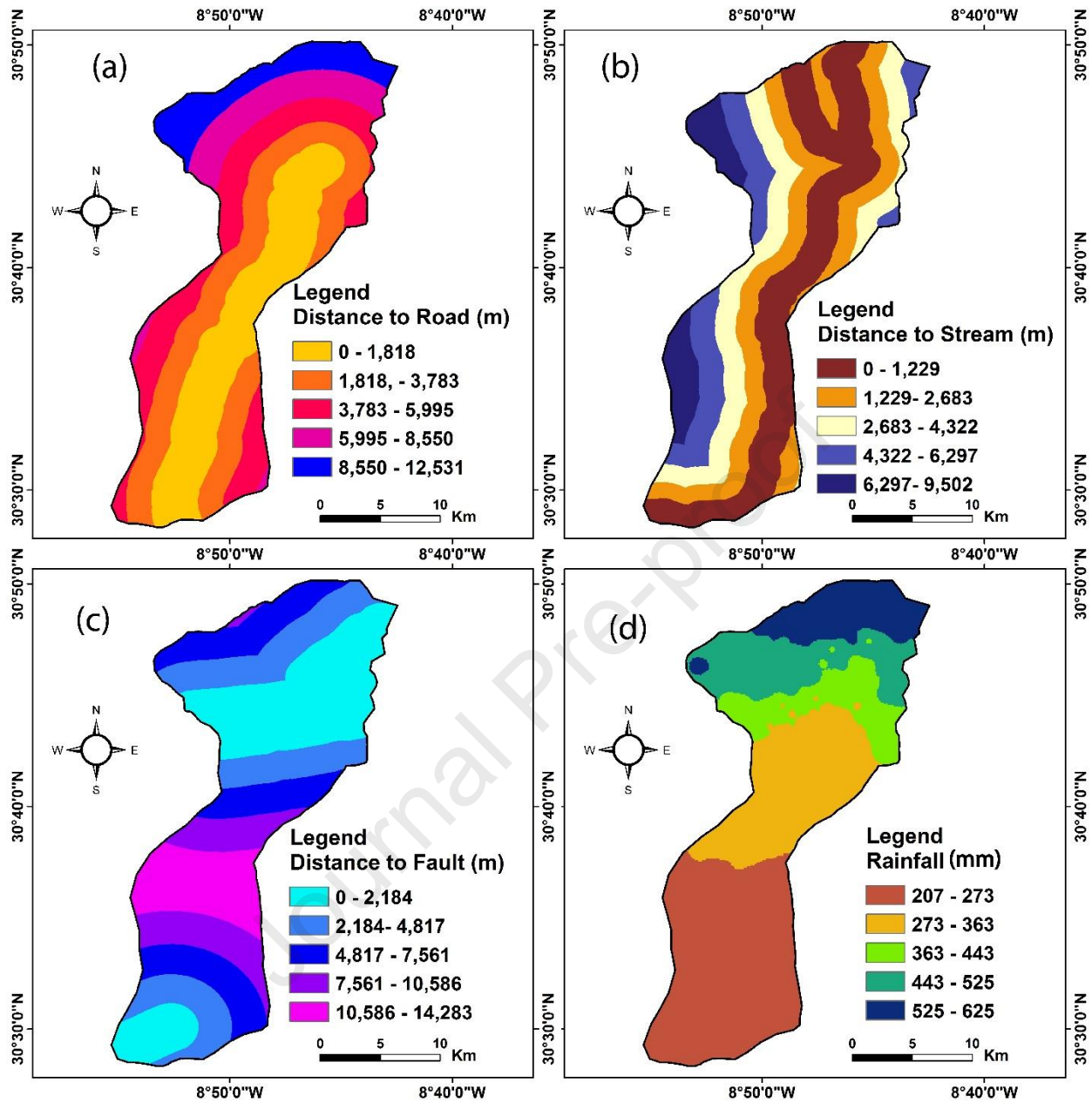


300

301

302

Fig. 6: Gully erosion conditioning factors: (a) Elevation, (b) Slope, (c) Aspect , and (d) Plan curvature.

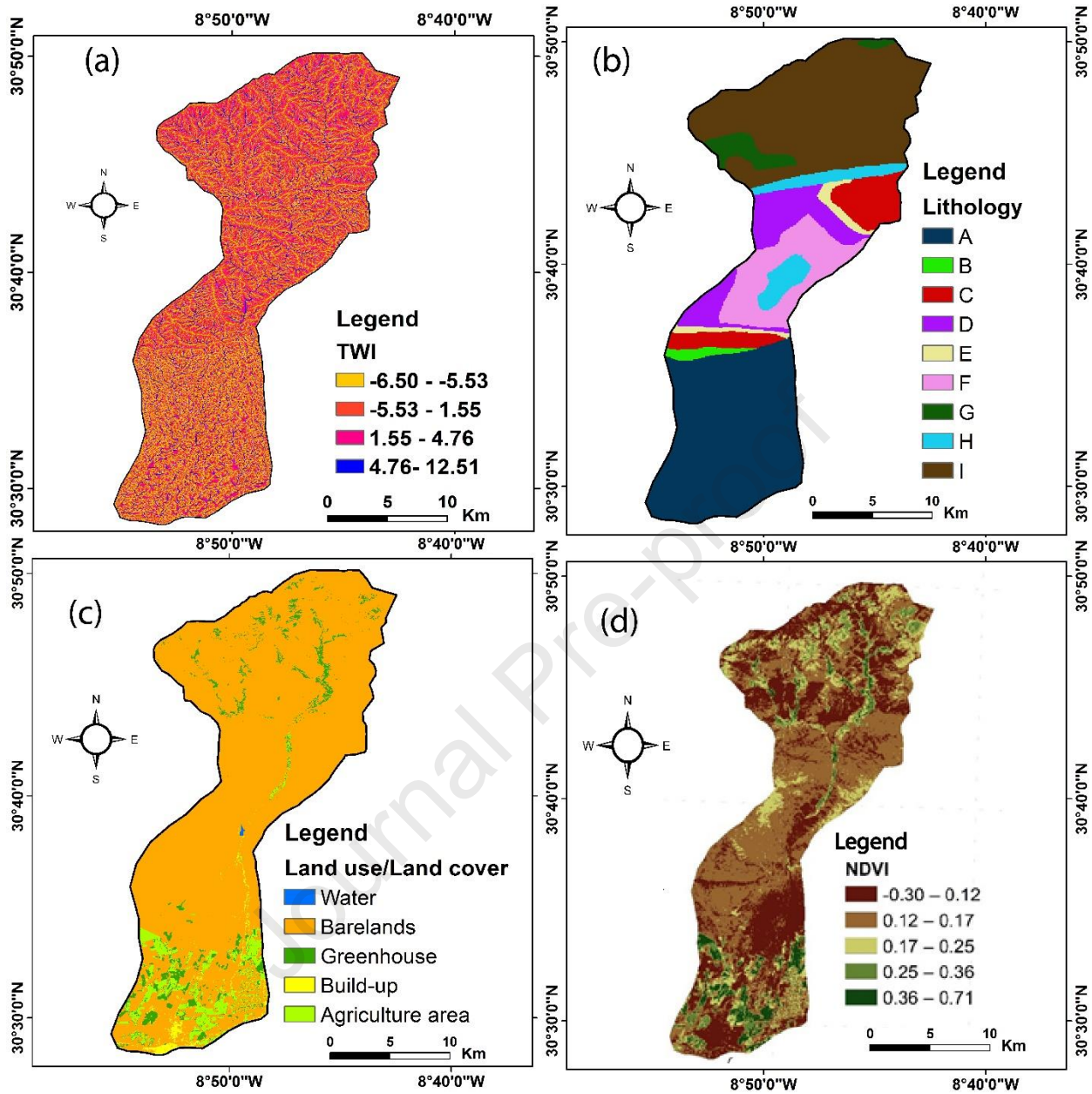


303

304

305

Fig. 7: Gully erosion conditioning factors: (a) Distance to road, (b) Distance to stream, (c) Distance to Faults and (d) Rainfall.



306

307 Fig. 8: Gully erosion conditioning factors: (a) TWI, (b) Lithology, (c) Land use/Land cover , and

308

(d) NDVI.

309 **4. Modelling process**310 **4.1. Multi-Layer Perceptron Neural Network (MLP NN)**

311 The MLP NN is an artificial neural network algorithm, widely used for classification approaches

312 (Roy and Saha, 2021). It consists of an input layer, hidden layer, and output layer. The hidden

313 layers process the data, while the output layers provide the classification results (Paola and
314 Schowengerdt, 1995). Connection weights between neurons are updated (Oliveira et al., 2015).
315 The main advantage of MLP is the non-dependency of prior assumptions of data distribution
316 (Gardner and Dorling, 1998). In this study, we considered 30 neurons and 2 hidden layers, the
317 Linear Unit Rectification (Relu) activation function, and the Adam optimizer (Adaptive Moment
318 Optimization) developed by (Kingma and Ba, 2017).

319 **4.2. Logistic Regression (LR)**

320 LR is a multivariate statistical model, used for fitting Bernoulli distributions (Arabameri et al.,
321 2018b). Unlike linear regression, logistic regression outcomes are binary or dichotomous (Hosmer
322 et al., 2000). The model describes the relationship between dependent and independent variables,
323 such as the presence or absence of gully erosion and the conditioning factors (Lucà et al., 2011).

324

4.3. K-Nearest Neighbours (KNN)

The KNN is a non-parametric model, considered one of the simplest machine learning algorithms (Zhang et al., 2018). The classification is based on the nearest neighbours. The number of neighbours (K) should be defined, which is used for the voting process (Abraham et al., 2021). The output consists of class membership likelihoods, according to Euclidean distance (Avand et al., 2019; Hussain et al., 2022). The most voted class is assigned to the analyzed data point. In this study, we select 8 nearest neighbours ($K=8$).

4.4. Random Forest (RF)

RF is a non-parametric ensemble learning algorithm that combines multiple decision tree models (Breiman, 2001). It randomly separated the input data into subsets for each internal decision tree (Quevedo et al., 2021). This study used the regression approach to generate numeric outcomes, for gully erosion susceptibility. The result is obtained by averaging the prediction of trees. RF also calculates the variable importance using mean decrease accuracy and mean decrease Gini index (Hitouri et al., 2022). In this study, 200 trees and 2 variables were selected for the main node split.

4.5. Weight of Evidence

The Weight of Evidence is a bivariate statistical test based on Bayesian probability (Bonham-Carter et al., 1988) that estimates the relative importance of each conditioning factor (Saha et al., 2020; Yang et al., 2021), using prior and posterior probability. The prior probability of gully erosion occurrence considers the number of pixels containing gully erosion and the total number of pixels in the study area (Pradhan et al., 2010). Then, positive and negative weights are calculated to identify the relationship between gully erosion conditioning factors and gully erosion occurrence. Finally, we calculate the standardized value of the difference to estimate the posterior probability relative certainty (Chen et al., 2018).

348 4.6. Modelling evaluation

349 The model performance assessment is used to determine and select the appropriate model for
 350 environmental hazards modelling (Chu et al., 2019; Lin and Chen, 2012; Pham et al., 2020). In
 351 this study, several statistical metrics widely used in previous studies were considered, including;
 352 AUC, specificity, sensitivity, and accuracy.

353 The ROC curve area (AUC) measures the performance of machine learning models. AUC values
 354 were classified into four precision categories, which are comprised between 0 and 1: poor (AUC
 355 = 0.6 to 0.7), fair (AUC = 0.7 to 0.8), good (AUC = 0.8–0.9), and excellent (AUC = 0.9–1)
 356 (Fressard et al., 2014). High values indicate a strong model, while low values mean a weak model
 357 (Hong et al., 2017). Overall accuracy (OA) represents the probability of occurrence of correctly
 358 classified pixels. It is calculated by the sum of true positive and true negative divided by all
 359 available singular tests (equation 7). Precision is used to measure the quality of the results. It is
 360 calculated by dividing the true positive by the sum of the true positive and false positive (equation
 361 8). Sensitivity is calculated by dividing the true-negative values by the sum of true negatives and
 362 false positives (equation 9) (Huang et al., 2023). Specificity represents the proportion of gully
 363 erosion pixels correctly predicted as gully erosion (equation 10).

$$364 \quad Accuracy = (TP + TN)/(TP + TN + FP + FN) \quad (6)$$

$$365 \quad Precision = TP/(TP + FP) \quad (7)$$

$$366 \quad Sensitivity = TP/(TP + FN) \quad (8)$$

$$367 \quad Specificity = TN/(TN + FP) \quad (9)$$

$$368 \quad AUC = X=1-specificity=1-(\frac{TP}{TN+FP}) \quad (10)$$

$$369 \quad Y = sensitivity = \frac{TP}{TP+FN}$$

370 Where TP represents true positive, TN represents true negative, FP represents false positive and
 371 FN represents false negative. The receiver operating characteristic (ROC) curve is represented
 372 through the AUC (Area Under the ROC curve), plotting sensitivity on the y-axis, and specificity
 373 on the x-axis.

374 4.7. Multicollinearity analysis

375 The multicollinearity test determines the relationship among the gully erosion conditioning
 376 factors and values the level of non-independence among them (Ghosh and Maiti, 2021). The
 377 presence of collinearity may generate bias in the modelling process and decrease the predictive
 378 performance (Arabameri et al., 2021). In this study, two indices were used: Tolerance (TOL) and
 379 Variance Inflation Factors (VIF), calculated as follows:

$$380 \quad TOL = 1 - R_i^2 \quad (11)$$

$$381 \quad VIF_i = \frac{1}{TOL} \quad (12)$$

382 Where R indicates the coefficient of determination of each conditioning factor i (O'brien, 2007).
 383 If the value of TOL is less than 0.1 and the value of VIF is greater than 10, collinearity exists
 384 amongst the variables. Table 2 represents the multicollinearity analysis of the gully erosion factors
 385 used.

386 **Table 2** Multi-collinearity among conditioning factors.

Factors	Collinearity Statistics	
	Tolerance	VIF
Elevation	0.427	2.341
Slope	0.881	1.135
Aspect	0.968	1.033
Lithology	0.718	1.393
Plan curvature	0.903	1.108
Distance to fault	0.910	1.098
Rainfall	0.414	2.413
Distance to stream	0.856	1.168

Distance to Road	0.920	1.087
TWI	0.967	1.034
NDVI	0.812	1.232
LULC	0.957	1.045

387

388 **5. Results**389 **5.1. Weight of evidence**

390 Table 3 represents the results of W_+ , W_- and the C_w , calculated for the 12 factors used in this
391 study. It is shown that: the greatest sensitivity to erosion has a slope in the range of 7.23° to 15.75°
392 ($C_w=1.857$), this confirms the interpretation that the phenomenon of erosion is less visible due to
393 the fact that some steeply sloping areas are made of very hard rocks (dolomites and limestones).
394 For the elevation, the most important class for erosion is the class; 792 m to 1.801, which is
395 characterized by $C_w= 2.201$. The greatest susceptibility to erosion is in the southwestern aspect
396 class ($C_w=0.316$). For the curvature plane, the strongest erosion factor is represented by the
397 concave land; the most erosion-sensitive class is between 792 m and 1801 m ($C_w= 1.849$). The
398 highest erosion sensitivity is observed when the distance to roads parameter is between 1818 m
399 and 3783 m ($C_w= 2.694$) and the distance to faults is between 4817 m and 7561 m ($C_w= 2.081$).
400 The highest sensitivity to erosion is observed when the TWI parameter is between 10.54 and 17.88
401 ($C_w= 0.8$) and the precipitation is between 273 mm and 363 mm ($C_w= 2.635$). For the lithology,
402 the maximum sensitivity to erosion was observed in the loose formations of Quaternary age in
403 class A ($C_w= 2.152$). The non-agricultural areas in Elouar watershed, represent the highest
404 vulnerability areas to erosion, due to the absence of vegetation. The LC/LU factor shows that the
405 building and construction areas in the study area represent the most erodible areas ($C_w= 4.513$).
406 The NDVI class most susceptible to erosion is characterized by index values between (-0.3) and
407 0.12 ($C_w= 2.833$). The high and very high frequency erodible areas were observed in the middle

408 and south of the El Ouaar watershed. The interpretation of the table shows that the higher the value
 409 of Cw, the more sensitive the class is to erosion, in consideration with the measurements of W+
 410 and W-.

411 **Table 3** WoE (C) values and factors affecting gully erosion.

Factors	Class/type	W+	W-	Cw
Slope	0-7.23	-1.411	0.465	-1.876
	7.23-15.75	1.297	-0.560	1.857
	15.75-24.79	0.435	-0.122	0.557
	24.79-35.13	-0.764	0.101	-0.865
	35.13-65.86	-0.764	0.047	-0.811
Elevation	214-792	-1.004	0.550	-1.554
	792-1,801	0.948	-1.254	2.201
	1,801-3,353	0.000	0.267	-0.267
Aspect	F	0.022	-0.003	0.025
	N	-0.878	0.078	-0.956
	NE	-0.360	0.053	-0.413
	E	-0.378	0.061	-0.439
	SE	-0.551	0.091	-0.642
	S	0.099	-0.020	0.119
	SW	0.264	-0.052	0.316
	W	-0.063	0.007	-0.070
	NW	-0.573	0.039	-0.612
Plan curvature	Concave	1.456	-0.393	1.849
	Flat	-1.227	1.457	-2.685
	Convex	0.651	-0.251	0.902
Distance to road	0-1,818	-1.554	0.346	-1.900
	1,818-3,783	1.652	-1.041	2.694
	3,783-5,995	-0.082	0.020	-0.102
	5,995-8,550	-1.042	0.091	-1.134
	8,550-12,531	0.000	0.148	-0.148
Distance to stream	0-1,229	-0.094	0.057	-0.152
	1,229-2,683	-0.204	0.081	-0.285
	2,683-4,322	-0.071	0.021	-0.092
	4,322-6,297	-0.490	0.078	-0.568
	6,297-9,502	-0.653	0.055	-0.708
Distance to fault	0-2,184	-0.309	0.144	-0.453
	2,184-4,817	-0.611	0.176	-0.786
	4,817-7,561	1.953	-0.128	2.081

	7,561-10,586	0.220	-0.046	0.266
	10,586-14,283	0.486	-0.114	0.601
TWI	10.54-17.88	0.714	-0.085	0.800
	17.88-19.63	0.455	-0.172	0.626
	19.63-21.30	0.436	-0.202	0.638
	21.30-29.07	0.592	-0.061	0.654
Rainfall	207-273	-1.218	0.451	-1.670
	273-363	1.904	-0.731	2.635
	363-443	1.032	-0.253	1.286
	443-525	0.000	0.267	-0.267
	525-625	0.000	0.167	-0.167
Lithology	A	2.071	-0.082	2.152
	B	0.000	-0.123	0.123
	C	0.000	-0.208	0.208
	D	0.000	-0.348	0.348
	E	0.000	-0.045	0.045
	F	0.000	-0.477	0.477
	G	0.000	0.004	-0.004
	H	0.000	-0.070	0.070
	I	0.000	0.041	-0.041
LC/LU	Water	0.000	0.000	0.000
	Greenhouse	0.196	-0.011	0.207
	Agriculture	0.689	-0.045	0.734
	Building/Construction	4.329	-0.184	4.513
	Soil	-0.262	1.083	-1.345
NDVI	(-0.3)-0.12	1.634	-1.199	2.833
	0.12-0.17	-1.333	0.474	-1.808
	0.17-0.25	-0.224	0.025	-0.249
	0.25-0.36	-0.199	0.009	-0.208
	0.36-0.71	-1.526	0.030	-1.556

412

413 **5.2. Gully erosion susceptibility mapping and models performance**

414 The gully erosion susceptibility of each model was classified into 5 classes: very low, low,
 415 moderate, high, and very high. The results were presented in Fig. 9 and Table 4.

416 The gully erosion susceptibility map developed using the RF model showed that 23.44% of the
 417 study area had very high erosion susceptibility, while 17.02%, 11.67%, 17.01%, and 30.85% of
 418 the area were classified as very low, low, moderate and high susceptibility, respectively.

419 For the MLP model, 28.39% of the area was classified as very high susceptibility, while 8.37%,
420 18.3%, 15.58%, and 29.37% had very low, low, moderate, and high susceptibilities, respectively.

421 For the KNN model, 27.64% of the study area was classified as very high gully risk, while 17.72%,
422 30.96%, 18.47%, and 5.21% had very low, low, moderate, and high sensitivities, For the LR model
423 19.66% of the study, the area was classified as very high gully, while 6.4%, 24.02%, 24.23%, and
424 25.69% had very low, low, moderate and high susceptibilities, respectively.

425 The spatial distribution of gully erosion susceptibility within this study area was quite similar for
426 all Machine Learning models developed here. These models show that the most eroded areas are
427 located in the southern part of Elouar watershed. These areas are characterized by a very high
428 intensity of erosion where the lithological formation is mainly dominated by poorly consolidated
429 quaternary deposits (silts and clays). These areas are characterized by a variation in slope, which
430 rapidly increases the transport of fine sediments in this area. In addition, inappropriate agricultural
431 practices and overgrazing of the area may also act as driving forces of gully erosion in the study
432 area. The northern part is characterized by less intense erosion than the southern part of this basin.
433 Indeed, this area is constituted by highly consolidated geological deposits which are represented
434 by limestones and dolomites (Ambroggi, 1963).

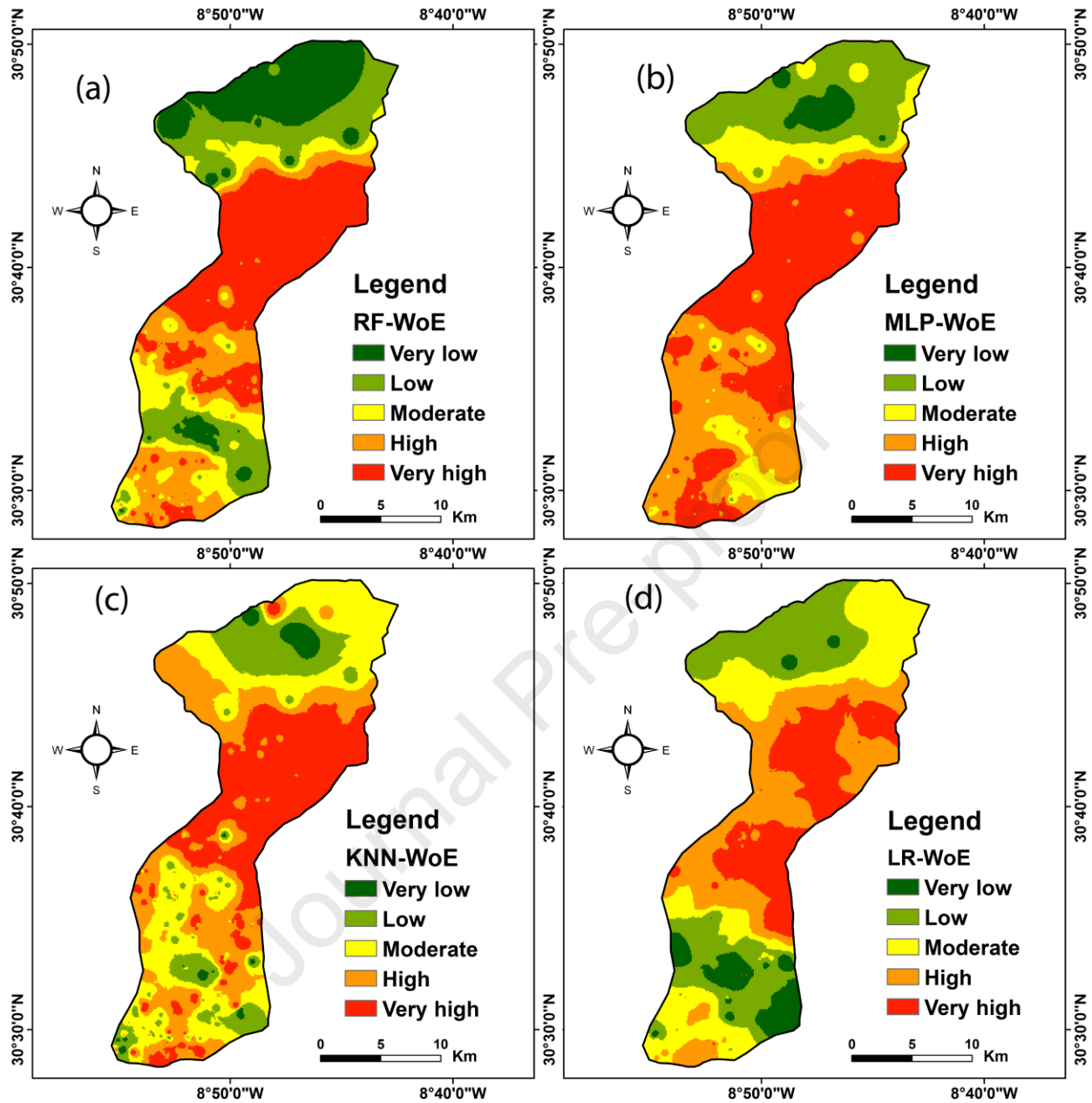
435 From a geomorphological point of view, the study area is part of the Souss plain which is located
436 between the High Atlas to the north and the Anti Atlas to the south, their geomorphological
437 position gives a great variation in the altitude, and for this reason the factors of erosion during
438 rainy periods are very intense. In addition, the intersection between the High Atlas and the Souss
439 plain shows a very strong water current and favours water erosion, and add to this, the sudden
440 succession of floods in the region during the past years.

441

442

443 **Table 4** Percentages of gully erosion susceptibility classes.

Models	% RF - WoE	% MLP- WoE	% KNN- WoE	% LR- WoE
Very low	23.44	8.37	5.21	6.40
Low	17.02	18.30	18.47	24.02
Moderate	11.67	15.58	30.96	24.23
High	17.01	29.37	17.72	25.69
Very high	30.85	28.39	27.64	19.66



444

445

Fig. 9: Gully erosion susceptibility mapping using: (a) RF-WOE, (b) MLP-WOE, (c) KNN-

446

WOE and LR-WOE.

447

448

449

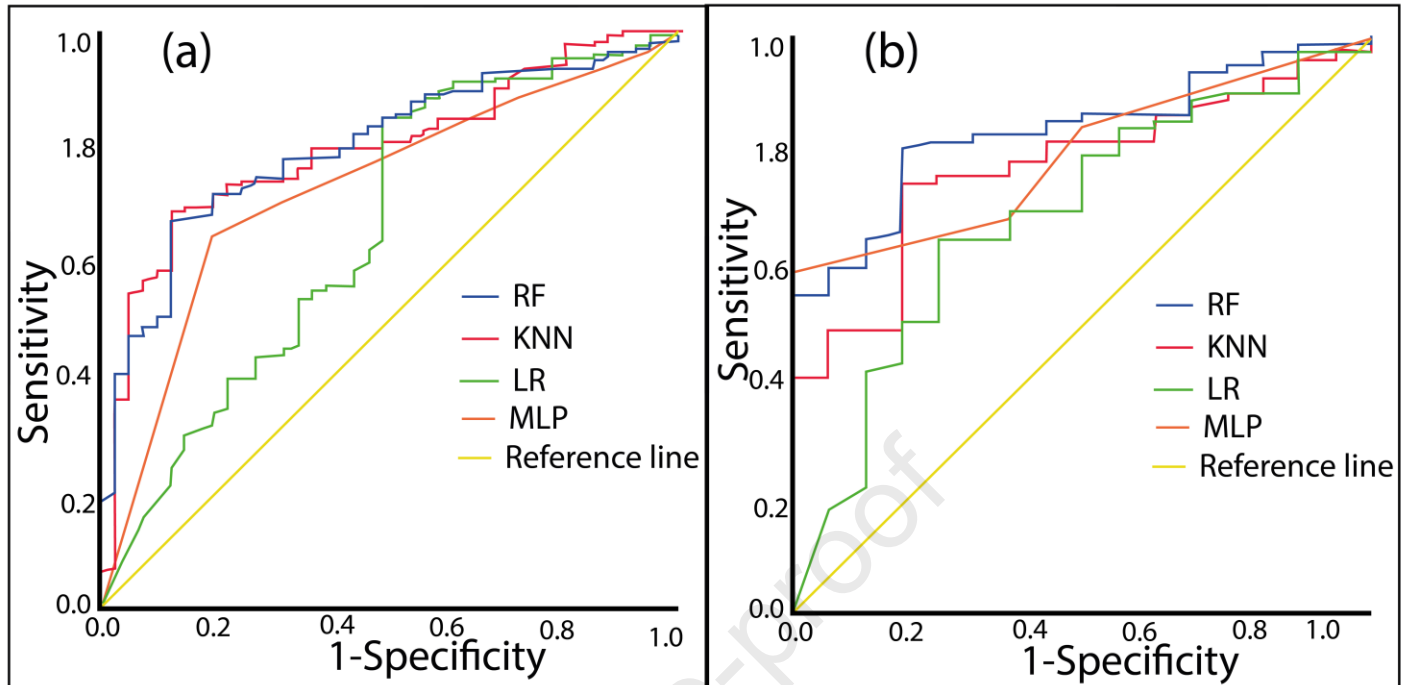


Fig. 10: (a) ROC curves of success rate and (b) ROC curves of prediction rate.

The performance of the developed models was evaluated using the receiver operating characteristic (ROC) curve analysis.

For RF model, the area under the curve (AUC) values are equals to 0.800 and 0.838 in the training and testing sets, respectively, as shown in Fig. 10.a and 10.b and Table 5. The model's accuracy of over 80% in the study area indicates that it is appropriate for mapping gully erosion susceptibility.

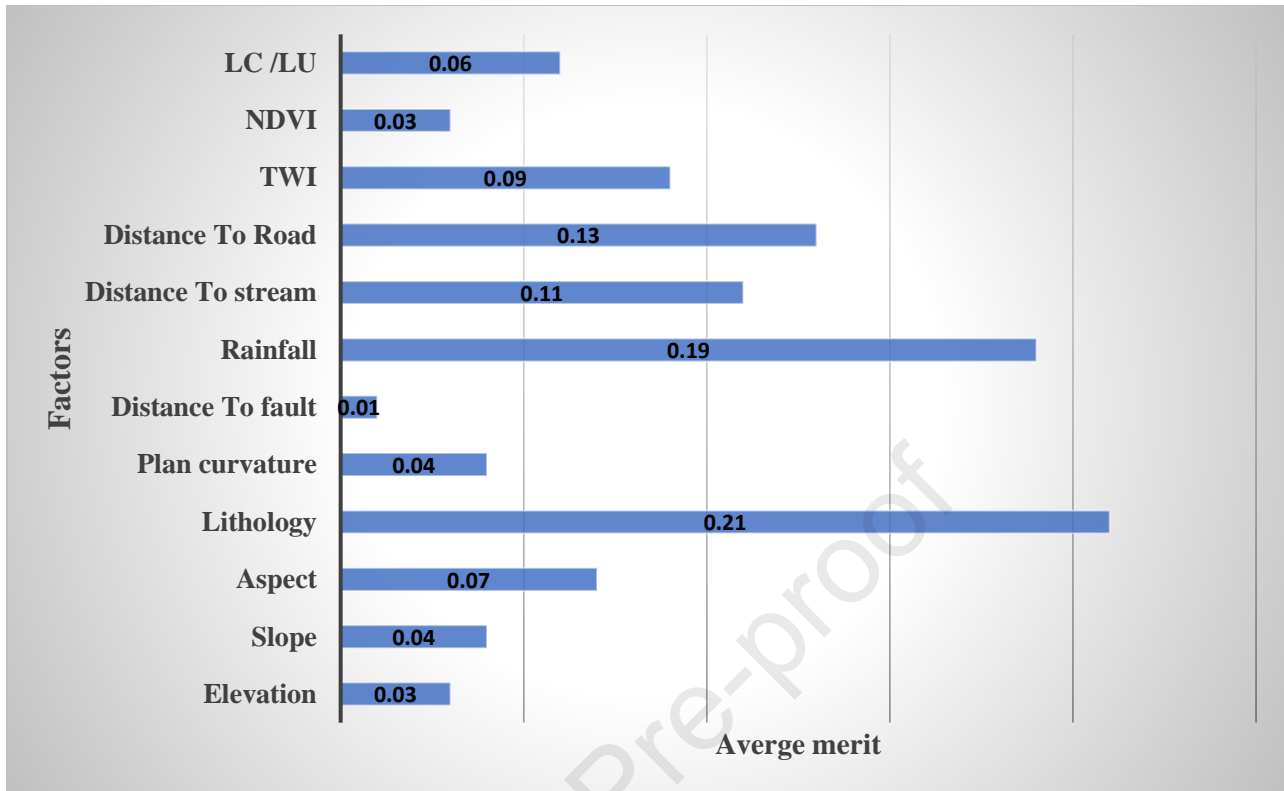
The accuracy of the classification models decreases in the following order: MLP, KNN, and LR with AUC of 0.796, 0.777, and 0.692, respectively, on the testing set. The study demonstrated that the RF model exhibited good performance in classification problems compared to other models, which is consistent with the findings of several previous studies (Avand et al., 2019; Rahmati et al., 2017; Saha et al., 2020).

464 **Table 5** Model statistical measures assigned to the training and testing datasets

	RF- WoE		MLP- WoE		KNN- WoE		LR- WoE	
	Training	Testing	Training	Testing	Training	Testing	Training	Testing
Accuracy	96.744	86.869	92.093	79.208	81.395	84.466	92.093	80.808
Precision	99.408	98.611	91.979	88.095	82.212	87.368	91.979	88.095
Sensitivity	96.552	85.542	98.851	87.059	98.276	95.402	98.851	89.157
Specificity	97.561	93.750	63.415	37.500	9.756	25.000	63.415	37.500
AUC	0.800	0.838	0.729	0.796	0.796	0.777	0.655	0.692

465

466 The RF model is a powerful and well-functioning model that has been demonstrated to be robust
467 and consistent with previous research. It is a sophisticated technique in spatial sciences that has
468 the ability to utilize multiple input variables and produce high accuracy predictions for various
469 classes. It has the ability to use explanatory variables and identify nonlinear relationships between
470 independent and dependent variables, making it a strong model for environmental hazard
471 assessment. Compared to other models, the RF model has the advantage of being able to handle
472 large datasets and manage numerous input variables efficiently. Its accurate machine learning
473 algorithms make it a highly accurate classifier for many datasets. In this study, the importance of
474 variables for gully erosion mapping for the El Ouair watershed was performed based on the RF
475 model. The variable importance values were LULC (0.06), NDVI (0.03), TWI (0.09), distance to
476 Road (0.13), distance to Stream (0.11), Rainfall (0.19), Distance to fault (0.01), Plan curvature
477 (0.04), Lithology (0.21), Aspect (0.07) and Slope (0.04) and Elevation (0.03). The most important
478 factors for gully susceptibility mapping in the Ouair watershed were lithology (0.21) and rainfall
479 (0.19), while distance to fault (0.01), was the least important (Fig. 11).



480

481

Fig. 11: The importance of conditioning factors.

482 6. Discussion

483 Gully erosion susceptibility models based on machine learning algorithms have been recognized
 484 as an effective tool for soil ecosystem management worldwide (Arabameri et al., 2021; Roy and
 485 Saha 2022; Wang et al., 2022) . In general, among other machine learning techniques, RF with its
 486 capacity to efficiently handle large datasets, non-linear parameters, categorical and continuous
 487 data, over-fitting, outliers, and multiple features was reported to produce the best performance in
 488 terms of high accuracy (Chen et al., 2021; Hembram et al., 2021; Lana et al., 2022; Pourghasemi
 489 et al., 2020; Saha et al., 2021)

490 The RF model has more precision than the other models, according to the results of this analysis,
 491 in creating a map of susceptibility to gully erosion (Fig. 10 and Table 5). An approach to modelling
 492 and analysing numerical data that includes both independent and dependent variables is called the

493 analysis of regression. In order to forecast the future behaviour of the dependent variable,
494 regression analysis aims to represent the dependent variable as an independent function of
495 variables, coefficients, and error values. When the link between the dependent and independent
496 variables is positive in certain areas of the research area and negative in other areas, it is obvious
497 that logistic regression cannot accurately and precisely detect the relationship.

498 This study, in agreement with recently published studies, also found that the RF algorithm is the
499 most suitable model for mapping gully erosion susceptibility in the El Ouair watershed based on
500 different performance criteria. Although several studies reported that other machine learning
501 models, for example, boosted regression tree (BRT) (Amiri et al., 2019) or extreme gradient
502 boosting (XGBoost) (Yang et al., 2021), generated better performance compared to the RF model,
503 the additional advantage of RF lies in its ability to evaluate the importance of each conditioning
504 factor in modelling process. This beneficial feature makes RF-based models widely used for
505 modelling processes in general and suitable for gully erosion susceptibility mapping in particular.
506 In addition, studies that better explain the model performance through the analysis of insight
507 mechanisms such as the distributions of variables and their interaction, rather than a pure
508 comparison based on the statistical criteria (e.g., RMSE and MAE), are strongly encouraged.

509 The present study indicated that lithology, rainfall, and distance to stream and road were the most
510 important variables influencing gully erosion susceptibility modelling. These findings are largely
511 in agreement with recent research (Rahmati et al., 2016; Amiri et al., 2019; Tien Bui et al., 2019;
512 Chen et al., 2021) where rainfall, lithology, and the distance from streams/rivers are generally
513 more important variables contributing to gully erosion than other conditioning factors. The results
514 from the four machine learning models used in this study also confirmed that the regions with
515 moderate rainfall, elevation, and slope but close to streams and roads are located in very high gully

516 erosion susceptibility areas. In contrast, the influence of LULC on gully erosion was found to be
517 not significantly strong (ranked 7th out of 12 variables) in this study. However, it is worth noting
518 that bare lands cover most of the study area. The results show a greater concentration of gully
519 erosion in areas with bare land in this study, which is in line with the report by Lei et al. (2020)
520 and Chen et al. (2020). The impact of land use/land cover on gully activity was also reported
521 previously (Vandekerckhove et al., 2003) ; nevertheless, there remain many doubts about the
522 features, such as mismanagement (Hosseinalizadeh et al., 2019) , that induce subsurface gully
523 development. Therefore, future research should explore further the uncertainties of LULC
524 variables in the development of gully erosion.

525 Recently, hybrid models based on the combination of two or more techniques have been highly
526 recommended for gully susceptibility prediction and mapping (Arabameri et al., 2020; Hitouri et
527 al., 2022; Roy and Saha 2022). This study also developed a hybrid machine learning model for
528 gully susceptibility prediction by integrating the Weight of Evidence (WoE) with Multilayer
529 Perceptron (MLP-WoE), Logistic Regression (LR-WoE), K-Nearest Neighbors (KNN-WoE) and
530 Random Forest (RF-WoE). While a comparison with stand-alone models was not performed by
531 the present study, other authors have reported that hybrid models can deliver better and perfect
532 results (Arabameri et al., 2020; Hembram et al., 2021). Tien Bui et al. (2019) proposed a hybrid
533 RF-ADTree model based on RF and alternating decision tree (ADTree) algorithms that were able
534 to significantly improve the prediction accuracy of the stand-alone ADTree model. Roy and Saha
535 (2022) also indicated that the integrated RSS-RBFnn and RTF-RBFnn models, i.e., radial basis
536 function neural network (RBFnn) combined with random sub-space (RSS) and rotation forest
537 (RTF), showed better results than the single RBFnn model for gully erosion susceptibility maps.
538 With the significant increase in the number of machine learning algorithms, future comparative

539 evaluations of single and hybrid models are important for the assessment of performance and
540 accuracy, since different modelling techniques may produce very different results and
541 performances. In addition, hybrid models developed from a combination with deep learning (Band
542 et al. 2020; Chen et al., 2021) can be promising studies of gully erosion susceptibility.

543 The geological and geographical situation of the Elouar watershed contribute to the risk of gully
544 erosion. Indeed, this watershed is part of the Souss Basin. The plain of this basin is filled with
545 recent Quaternary deposits, consisting of loose to semi-compact layers that are sensitive to erosion.
546 These deposits are composed of lithostratigraphic units U1 to U4 mentioned above (Aït Hssaine,
547 1994; Ambroggi, 1963; Hssaisoune et al., 2012). Climate factors also play an important role in this
548 area. The study area is characterized by an arid and semi-arid climate, influenced by the
549 geographical location, especially the High Atlas Mountains to the north, the Anti-Atlas Mountains
550 to the south, and the Atlantic Ocean to the east. The variation in rainfall between the north and
551 south promotes strong water currents in the rivers due to the altitude difference between the
552 upstream area of the study area, which can reach over 3000 meters, and its downstream area, which
553 can be as low as 194 meters, facilitating water transport and contributing to the gully erosion risks.
554 Overgrazing and anthropogenic factors also contribute to erosion risks in this area, and laws should
555 be enacted to regulate irresponsible land use practices. The effect of this phenomenon is manifested
556 in the destruction of infrastructure (roads, bridges, houses...), which results in significant material
557 and economic losses for the country. For instance, the Faculty of Sharia and Law in Taroudant,
558 constructed in a highly area-prone to erosion by ravines, has led to the destruction of walls and the
559 emergence of erosive areas both inside and outside of the faculty (Fig. 12).



560

561 Fig. 12: Photos showing the influence of gully erosion on the infrastructure within the study area.

562 To minimize this influence, several measures have been taken to address the issue of gully erosion
563 in the Taroudant region. These include the construction of walls along the banks of the Elouar river
564 and the gullies that are particularly prone to erosion. Additionally, the construction of sidewalks
565 next to roads and the implementation of greenhouse agriculture have also been considered as part
566 of the actions to mitigate and overcome the spread of this phenomenon (Fig. 13).



567

568 Fig. 13: Photos showing some solutions implemented to prevent the distribution of gully erosion
569 in the study area.

570 In this context, our study underscores the critical importance of the developed models in the field
571 of gully erosion mapping. However, we recognize that there is a room for improvement in future
572 research. For instance, in our study, we based on freely available GIS data due to the lack of high-
573 resolution datasets. We acknowledge that this choice of data has certain limitations, specifically
574 regarding data resolution for controlling factors, which resulted in the low accuracy and low
575 precision of the developed models. It should be noted that accurate and detailed gully erosion
576 requires high spatial resolutions (Garosi et al., 2018; Rahmati et al., 2016). In addition, it is

577 essential to highlight the significance of data quality and recognizing the uncertainties associated
578 with using controlling factors with different pixel sizes is of utmost importance. Although many
579 studies have investigated the susceptibility of gully erosion based on different pixel size of some
580 controlling factors (Garosi et al., 2018; Rahmati et al., 2016). There is still ongoing debate
581 regarding the most appropriate pixel size to consider when examining controlling factors for gully
582 mapping susceptibility.

583 **7. Conclusion**

584 In conclusion, this study successfully achieved its goal of using multi-collinearity analysis to
585 identify significant factors in gully erosion, creating hybrid machine learning models to map
586 erosion-prone areas, employing k-fold cross-validation to mitigate randomness, and assessing the
587 capability and robustness of the models using ROC. This study shows that the weight of evidence
588 is very important in identifying the most suitable conditioning factors to generate an effective map
589 of gully erosion susceptibility in the El Ouaar watershed. The results showed that RF-WoE
590 obtained the best performance (AUC = 0.8), followed by KNN-WoE (AUC = 0.796), then MLP-
591 WoE (AUC = 0.729) and LP-WoE (AUC = 0.655), respectively. These results showed that the
592 good precision obtained is due to the fact that each type of erosion has its own set of conditioning
593 factors, which must be evaluated separately. The results obtained from this work provide planners
594 and researchers with an appropriate perspective on the effect of conditioning factors in future
595 analysis. Further research could explore the use of other machine learning techniques and consider
596 additional factors to improve the accuracy of gully erosion prediction models.

597 **Ethical Approval:** Not applicable

598 **Consent to Participate:** Not applicable

599 **Consent to Publish:** Not applicable

600 **Funding:** No external funding

601 **Competing Interests:** This manuscript has not been published or presented elsewhere in part or
602 entirety and is not under consideration by another journal. There are no conflicts of interest to
603 declare.

604 **Acknowledgement:** The authors are thankful to the Deanship of Scientific Research at Najran
605 University for funding this work, under the Research Groups Funding program grant code
606 (NU/RG/SERC/12/21).

607 **Availability of data and materials:** The data that support the findings of this study are available
608 from the corresponding author upon reasonable request.

609 **References**

- 610 Abraham, M.T., Satyam, N., Lokesh, R., Pradhan, B., Alamri, A., 2021. Factors affecting
611 landslide susceptibility mapping: Assessing the influence of different machine learning
612 approaches, sampling strategies and data splitting. *Land* 10, 989.
- 613 Abu El-Magd, S.A., Ali, S.A., Pham, Q.B., 2021. Spatial modeling and susceptibility zonation of
614 landslides using random forest, naïve bayes and K-nearest neighbor in a complicated
615 terrain. *Earth Science Informatics* 14, 1227–1243.
- 616 Aït Hssaïne, A., 1994. Géomorphologie et Quaternaire du piémont de Taroudant-Ouled Teïma,
617 Maroc (PhD Thesis). Thèse inédite, université de Montréal.
- 618 Ajit, P., 2016. Prediction of employee turnover in organizations using machine learning
619 algorithms. *algorithms* 4, C5.
- 620 Ali, S.A., Parvin, F., Pham, Q.B., Khedher, K.M., Dehbozorgi, M., Rabby, Y.W., Anh, D.T.,
621 Nguyen, D.H., 2022. An ensemble random forest tree with SVM, ANN, NBT, and LMT
622 for landslide susceptibility mapping in the Rangit River watershed, India. *Natural*
623 *Hazards* 1–33.
- 624 Ali, S.A., Parvin, F., Pham, Q.B., Vojtek, M., Vojteková, J., Costache, R., Linh, N.T.T., Nguyen,
625 H.Q., Ahmad, A., Ghorbani, M.A., 2020. GIS-based comparative assessment of flood
626 susceptibility mapping using hybrid multi-criteria decision-making approach, naïve
627 Bayes tree, bivariate statistics and logistic regression: a case of Topl'a basin, Slovakia.
628 *Ecological Indicators* 117, 106620.
- 629 Ali, S.A., Parvin, F., Vojteková, J., Costache, R., Linh, N.T.T., Pham, Q.B., Vojtek, M., Gigović,
630 L., Ahmad, A., Ghorbani, M.A., 2021. GIS-based landslide susceptibility modeling: A
631 comparison between fuzzy multi-criteria and machine learning algorithms. *Geoscience*
632 *Frontiers* 12, 857–876.

- 633 Amare, S., Langendoen, E., Keesstra, S., Ploeg, M. van der, Gelagay, H., Lemma, H., Zee, S.E.
634 van der, 2021. Susceptibility to gully erosion: applying random forest (RF) and frequency
635 ratio (FR) approaches to a small catchment in Ethiopia. *Water* 13, 216.
- 636 Ambroggi, R., 1963. Etude géologique du versant méridional du Haut Atlas occidental et de la
637 plaine du Souss. Editions marocaines et internationales.
- 638 Amiri, M., Pourghasemi, H.R., Ghanbarian, G.A., Afzali, S.F., 2019. Assessment of the
639 importance of gully erosion effective factors using Boruta algorithm and its spatial
640 modeling and mapping using three machine learning algorithms. *Geoderma* 340, 55–69.
- 641 Arabameri, A., Cerda, A., Tiefenbacher, J.P., 2019. Spatial pattern analysis and prediction of
642 gully erosion using novel hybrid model of entropy-weight of evidence. *Water* 11, 1129.
- 643 Arabameri, A., Chandra Pal, S., Costache, R., Saha, A., Rezaie, F., Seyed Danesh, A., Pradhan,
644 B., Lee, S., Hoang, N.-D., 2021. Prediction of gully erosion susceptibility mapping using
645 novel ensemble machine learning algorithms. *Geomatics, Natural Hazards and Risk* 12,
646 469–498.
- 647 Arabameri, A., Pradhan, B., Rezaei, K., Yamani, M., Pourghasemi, H.R., Lombardo, L., 2018a.
648 Spatial modelling of gully erosion using evidential belief function, logistic regression,
649 and a new ensemble of evidential belief function–logistic regression algorithm. *Land
650 Degradation & Development* 29, 4035–4049.
- 651 Arabameri, A., Rezaei, K., Pourghasemi, H.R., Lee, S., Yamani, M., 2018b. GIS-based gully
652 erosion susceptibility mapping: a comparison among three data-driven models and AHP
653 knowledge-based technique. *Environmental earth sciences* 77, 1–22.
- 654 Arabameri, A., Saha, S., Roy, J., Tiefenbacher, J.P., Cerda, A., Biggs, T., Pradhan, B., Thi Ngo,
655 P.T., Collins, A.L., 2020. A novel ensemble computational intelligence approach for the
656 spatial prediction of land subsidence susceptibility. *Science of The Total Environment*
657 726, 138595. <https://doi.org/10.1016/j.scitotenv.2020.138595>
- 658 Avand, M., Janizadeh, S., Naghibi, S.A., Pourghasemi, H.R., Khosrobeigi Bozchaloei, S.,
659 Blaschke, T., 2019. A comparative assessment of random forest and k-nearest neighbor
660 classifiers for gully erosion susceptibility mapping. *Water* 11, 2076.
- 661 Azareh, A., Rahmati, O., Rafiei-Sardooi, E., Sankey, J.B., Lee, S., Shahabi, H., Ahmad, B.B.,
662 2019. Modelling gully-erosion susceptibility in a semi-arid region, Iran: Investigation of
663 applicability of certainty factor and maximum entropy models. *Science of the Total
664 Environment* 655, 684–696.
- 665 Azedou, A., Lahssini, S., Khattabi, A., Meliho, M., Rifai, N., 2021. A methodological
666 comparison of three models for gully erosion susceptibility mapping in the rural
667 municipality of El Faïd (Morocco). *Sustainability* 13, 682.
- 668 Band, S.S., Janizadeh, S., Chandra Pal, S., Saha, A., Chakraborty, R., Shokri, M., Mosavi, A.,
669 2020. Novel ensemble approach of deep learning neural network (DLNN) model and
670 particle swarm optimization (PSO) algorithm for prediction of gully erosion
671 susceptibility. *Sensors* 20, 5609.

- 672 Belasri, A., Lakhouili, A., 2016. Estimation of soil erosion risk using the universal soil loss
673 equation (USLE) and geo-information technology in Oued El Makhazine Watershed,
674 Morocco. *Journal of Geographic Information System* 8, 98.
- 675 Belayneh, M., Yirgu, T., Tsegaye, D., 2020. Current extent, temporal trends, and rates of gully
676 erosion in the Gumara watershed, Northwestern Ethiopia. *Global Ecology and*
677 *Conservation* 24, e01255.
- 678 Bilotta, G.S., Brazier, R.E., Haygarth, P.M., 2007. The impacts of grazing animals on the quality
679 of soils, vegetation, and surface waters in intensively managed grasslands. *Advances in*
680 *agronomy* 94, 237–280.
- 681 Bonham-Carter, G.F., Agterberg, F.P., Wright, D.F., 1988. Integration of geological datasets for
682 gold exploration in Nova Scotia. *Photogrammetric Engineering and Remote Sensing* 54,
683 1585–1592.
- 684 Bouslihim, Y., 2020. Hydrological and soil erosion modeling using SWAT model and
685 Pedotransfert Functions: A case study of Settat-Ben Ahmed watersheds, Morocco (PhD
686 Thesis). Université Hassan Ier Settat (Maroc).
- 687 Breiman, L., 2001. Random forests. *Machine learning* 45, 5–32.
- 688 Chakraborty, R., Pal, S.C., 2023. Systematic review on gully erosion measurement, modelling
689 and management: Mitigation alternatives and policy recommendations. *Geological*
690 *Journal*.
- 691 Chen, W., Lei, X., Chakraborty, R., Pal, S.C., Sahana, M., Janizadeh, S., 2021. Evaluation of
692 different boosting ensemble machine learning models and novel deep learning and
693 boosting framework for head-cut gully erosion susceptibility. *Journal of Environmental*
694 *Management* 284, 112015.
- 695 Chen, W., Li, H., Hou, E., Wang, S., Wang, G., Panahi, M., Li, T., Peng, T., Guo, C., Niu, C.,
696 Xiao, L., Wang, J., Xie, X., Ahmad, B. Bin, 2018. GIS-based groundwater potential
697 analysis using novel ensemble weights-of-evidence with logistic regression and
698 functional tree models. *Science of The Total Environment* 634, 853–867.
699 <https://doi.org/10.1016/j.scitotenv.2018.04.055>
- 700 Chen, Y., Qin, S., Qiao, S., Dou, Q., Che, W., Su, G., Yao, J., Nnanwuba, U.E., 2020. Spatial
701 predictions of debris flow susceptibility mapping using convolutional neural networks in
702 Jilin Province, China. *Water* 12, 2079.
- 703 Choubin, B., Moradi, E., Golshan, M., Adamowski, J., Sajedi-Hosseini, F., Mosavi, A., 2019. An
704 ensemble prediction of flood susceptibility using multivariate discriminant analysis,
705 classification and regression trees, and support vector machines. *Science of the Total*
706 *Environment* 651, 2087–2096.
- 707 Chu, L., Wang, L.-J., Jiang, J., Liu, X., Sawada, K., Zhang, J., 2019. Comparison of landslide
708 susceptibility maps using random forest and multivariate adaptive regression spline
709 models in combination with catchment map units. *Geosciences Journal* 23, 341–355.

- 710 Conforti, M., Aucelli, P.P., Robustelli, G., Scarciglia, F., 2011. Geomorphology and GIS
711 analysis for mapping gully erosion susceptibility in the Turbolo stream catchment
712 (Northern Calabria, Italy). *Natural hazards* 56, 881–898.
- 713 Conoscenti, C., Angileri, S., Cappadonia, C., Rotigliano, E., Agnesi, V., Märker, M., 2014. Gully
714 erosion susceptibility assessment by means of GIS-based logistic regression: A case of
715 Sicily (Italy). *Geomorphology* 204, 399–411.
716 <https://doi.org/10.1016/j.geomorph.2013.08.021>
- 717 Davis, C.R., Trevatt, A.E., McGoldrick, R.B., Parrott, F.E., Mohanna, P.-N., 2016. How to train
718 plastic surgeons of the future. *Journal of Plastic, Reconstructive & Aesthetic Surgery* 69,
719 1134–1140.
- 720 Dijon, R., 1966. Reconnaissance hydrogéologique et ressources en eau du bassin des oueds
721 Seyad-Ouarg-Noun, Maroc Sud-occidental (PhD Thesis). Montpellier.
- 722 d'Oleire-Oltmanns, S., Marzloff, I., Tiede, D., Blaschke, T., 2014. Detection of gully-affected
723 areas by applying object-based image analysis (OBIA) in the region of Taroudannt,
724 Morocco. *Remote Sensing* 6, 8287–8309.
- 725 Elmoulat, M., Ait Brahim, L., 2018. Landslides susceptibility mapping using GIS and weights of
726 evidence model in Tetouan-Ras-Mazari area (Northern Morocco). *Geomatics, Natural
727 Hazards and Risk* 9, 1306–1325.
- 728 Fressard, M., Thiery, Y., Maquaire, O., 2014. Which data for quantitative landslide susceptibility
729 mapping at operational scale? Case study of the Pays d'Auge plateau hillslopes
730 (Normandy, France). *Natural Hazards and Earth System Sciences* 14, 569–588.
731 <https://doi.org/10.5194/nhess-14-569-2014>
- 732 Gafurov, A.M., Yermolayev, O.P., 2020. Automatic gully detection: Neural networks and
733 computer vision. *Remote Sensing* 12, 1743.
- 734 Gardner, M.W., Dorling, S.R., 1998. Artificial neural networks (the multilayer perceptron)—a
735 review of applications in the atmospheric sciences. *Atmospheric environment* 32, 2627–
736 2636.
- 737 Garosi, Y., Sheklabadi, M., Pourghasemi, H.R., Besalatpour, A.A., Conoscenti, C., Van Oost, K.,
738 2018. Comparison of differences in resolution and sources of controlling factors for gully
739 erosion susceptibility mapping. *Geoderma* 330, 65–78.
- 740 Ghorbani Nejad, S., Falah, F., Daneshfar, M., Haghizadeh, A., Rahmati, O., 2017. Delineation of
741 groundwater potential zones using remote sensing and GIS-based data-driven models.
742 *Geocarto international* 32, 167–187.
- 743 Ghorbanzadeh, O., Blaschke, T., Aryal, J., Gholaminia, K., 2020a. A new GIS-based technique
744 using an adaptive neuro-fuzzy inference system for land subsidence susceptibility
745 mapping. *Journal of Spatial Science* 65, 401–418.
746 <https://doi.org/10.1080/14498596.2018.1505564>
- 747 Ghorbanzadeh, O., Shahabi, H., Mirchooli, F., Valizadeh Kamran, K., Lim, S., Aryal, J.,
748 Jarihani, B., Blaschke, T., 2020b. Gully erosion susceptibility mapping (GESM) using

- 749 machine learning methods optimized by the multi-collinearity analysis and K-fold cross-
750 validation. *Geomatics, Natural Hazards and Risk* 11, 1653–1678.
- 751 Ghorbanzadeh, O., Valizadeh Kamran, K., Blaschke, T., Aryal, J., Naboureh, A., Einali, J., Bian,
752 J., 2019. Spatial prediction of wildfire susceptibility using field survey gps data and
753 machine learning approaches. *Fire* 2, 43.
- 754 Ghosh, A., Maiti, R., 2021. Soil erosion susceptibility assessment using logistic regression,
755 decision tree and random forest: study on the Mayurakshi river basin of Eastern India.
756 *Environmental Earth Sciences* 80, 1–16.
- 757 Golestani, G., Issazadeh, L., Serajamani, R., 2014. Lithology effects on gully erosion in Ghoori
758 chay Watershed using RS & GIS. *Int. J. Biosci* 4, 71–76.
- 759 Gomiero, T., 2016. Soil degradation, land scarcity and food security: Reviewing a complex
760 challenge. *Sustainability* 8, 281.
- 761 Hancock, G.R., Evans, K.G., 2010. Gully, channel and hillslope erosion—an assessment for a
762 traditionally managed catchment. *Earth surface processes and landforms* 35, 1468–1479.
- 763 Hembram, T.K., Saha, S., Pradhan, B., Abdul Maulud, K.N., Alamri, A.M., 2021. Robustness
764 analysis of machine learning classifiers in predicting spatial gully erosion susceptibility
765 with altered training samples. *Geomatics, Natural Hazards and Risk* 12, 794–828.
766 <https://doi.org/10.1080/19475705.2021.1890644>
- 767 Hitouri, S., Varasano, A., Mohajane, M., Ijlil, S., Essahlaoui, N., Ali, S.A., Essahlaoui, A.,
768 Pham, Q.B., Waleed, M., Palateerdham, S.K., 2022. Hybrid Machine Learning Approach
769 for Gully Erosion Mapping Susceptibility at a Watershed Scale. *ISPRS International*
770 *Journal of Geo-Information* 11, 401.
- 771 Hong, H., Naghibi, S.A., Moradi Dashtpajardi, M., Pourghasemi, H.R., Chen, W., 2017. A
772 comparative assessment between linear and quadratic discriminant analyses (LDA-QDA)
773 with frequency ratio and weights-of-evidence models for forest fire susceptibility
774 mapping in China. *Arabian Journal of Geosciences* 10, 1–14.
- 775 Hosmer, D.W., Lemeshow, S., Sturdivant, R.X., 2000. Introduction to the logistic regression
776 model. *Applied logistic regression* 2, 1–30.
- 777 Hosseinalizadeh, M., Kariminejad, N., Chen, W., Pourghasemi, H.R., Alinejad, M., Behbahani,
778 A.M., Tiefenbacher, J.P., 2019. Gully headcut susceptibility modeling using functional
779 trees, naïve Bayes tree, and random forest models. *Geoderma* 342, 1–11.
- 780 Hssaisoune, M., Boutaleb, S., Benssaou, M., Tagma, T., Fasskaoui, M.E., Bouchaou, L., 2012.
781 Analyse géophysique et structurale de l'aquifère de la plaine du Souss-Massa: synthèse et
782 conséquences hydrogéologiques 20.
- 783 Huang, D., Su, L., Zhou, L., Tian, Y., Fan, H., 2023. Assessment of gully erosion susceptibility
784 using different DEM-derived topographic factors in the black soil region of Northeast
785 China. *International Soil and Water Conservation Research* 11, 97–111.
786 <https://doi.org/10.1016/j.iswcr.2022.04.001>
- 787 Hughes, A., Prosser, I., Stevenson, J., Scott, A., Lu, H., Gallant, J., Moran, C., 2001. Gully
788 Erosion Mapping for the National Land and Water Resources Audit.

- 789 Hussain, M.A., Chen, Z., Kalsoom, I., Asghar, A., Shoaib, M., 2022. Landslide Susceptibility
790 Mapping Using Machine Learning Algorithm: A Case Study Along Karakoram Highway
791 (KKH), Pakistan. *J Indian Soc Remote Sens* 50, 849–866.
792 <https://doi.org/10.1007/s12524-021-01451-1>
- 793 Issaka, S., Ashraf, M.A., 2017. Impact of soil erosion and degradation on water quality: a review.
794 *Geology, Ecology, and Landscapes* 1, 1–11.
- 795 Jaafari, A., Janizadeh, S., Abdo, H.G., Mafi-Gholami, D., Adeli, B., 2022. Understanding land
796 degradation induced by gully erosion from the perspective of different geoenvironmental
797 factors. *Journal of Environmental Management* 315, 115181.
- 798 Jiang, C., Fan, W., Yu, N., Nan, Y., 2021. A new method to predict gully head erosion in the
799 Loess Plateau of China based on SBAS-InSAR. *Remote Sensing* 13, 421.
- 800 Karami, A., Khorani, A., Noohegar, A., Shamsi, S.R.F., Moosavi, V., 2015. Gully Erosion
801 Mapping Using Object-Based and Pixel-Based Image Classification Methods Gully
802 Erosion Mapping. *Environmental & Engineering Geoscience* 21, 101–110.
- 803 Kingma, D.P., Ba, J., 2017. Adam: A Method for Stochastic Optimization.
- 804 Lana, J.C., Castro, P. de T.A., Lana, C.E., 2022. Assessing gully erosion susceptibility and its
805 conditioning factors in southeastern Brazil using machine learning algorithms and
806 bivariate statistical methods: A regional approach. *Geomorphology* 402, 108159.
807 <https://doi.org/10.1016/j.geomorph.2022.108159>
- 808 Lei, X., Chen, W., Avand, M., Janizadeh, S., Kariminejad, N., Shahabi, Hejar, Costache, R.,
809 Shahabi, Himan, Shirzadi, A., Mosavi, A., 2020. GIS-based machine learning algorithms
810 for gully erosion susceptibility mapping in a semi-arid region of Iran. *Remote Sensing*
811 12, 2478.
- 812 Lin, G.-W., Chen, H., 2012. The relationship of rainfall energy with landslides and sediment
813 delivery. *Engineering geology* 125, 108–118.
- 814 Lucà, F., Conforti, M., Robustelli, G., 2011. Comparison of GIS-based gully susceptibility
815 mapping using bivariate and multivariate statistics: Northern Calabria, South Italy.
816 *Geomorphology* 134, 297–308.
- 817 Meliho, M., Khatibi, A., Mhammdi, N., 2018. A GIS-based approach for gully erosion
818 susceptibility modelling using bivariate statistics methods in the Ourika watershed,
819 Morocco. *Environmental Earth Sciences* 77, 1–14.
- 820 Merghadi, A., Yunus, A.P., Dou, J., Whiteley, J., ThaiPham, B., Bui, D.T., Avtar, R.,
821 Abderrahmane, B., 2020. Machine learning methods for landslide susceptibility studies:
822 A comparative overview of algorithm performance. *Earth-Science Reviews* 207, 103225.
- 823 Mohsin, M., Ali, S.A., Shamim, S.K., Ahmad, A., 2022. A GIS-based novel approach for
824 suitable sanitary landfill site selection using integrated fuzzy analytic hierarchy process
825 and machine learning algorithms. *Environmental Science and Pollution Research* 29,
826 31511–31540.

- 827 Momm, H.G., Bingner, R.L., Wells, R.R., Wilcox, D., 2012. AGNPS GIS-based tool for
828 watershed-scale identification and mapping of cropland potential ephemeral gullies.
829 *Applied engineering in agriculture* 28, 17–29.
- 830 Moore, I.D., Grayson, R.B., Ladson, A.R., 1991. Digital terrain modelling: a review of
831 hydrological, geomorphological, and biological applications. *Hydrological processes* 5,
832 3–30.
- 833 Moore, I.D., Wilson, J.P., 1992. Length-slope factors for the Revised Universal Soil Loss
834 Equation: Simplified method of estimation. *Journal of soil and water conservation* 47,
835 423–428.
- 836 Mosaid, H., Barakat, A., Bustillo, V., Rais, J., 2022. Modeling and Mapping of Soil Water
837 Erosion Risks in the Srou Basin (Middle Atlas, Morocco) Using the EPM Model, GIS
838 and Magnetic Susceptibility. *Journal of Landscape Ecology* 15, 126–147.
- 839 Nhu, V.-H., Shirzadi, A., Shahabi, H., Singh, S.K., Al-Ansari, N., Clague, J.J., Jaafari, A., Chen,
840 W., Miraki, S., Dou, J., 2020. Shallow landslide susceptibility mapping: A comparison
841 between logistic model tree, logistic regression, naïve bayes tree, artificial neural
842 network, and support vector machine algorithms. *International journal of environmental
843 research and public health* 17, 2749.
- 844 Nir, N., Knitter, D., Hardt, J., Schütt, B., 2021. Human movement and gully erosion:
845 Investigating feedback mechanisms using Frequency Ratio and Least Cost Path analysis
846 in Tigray, Ethiopia. *PloS one* 16, e0245248.
- 847 O'brien, R.M., 2007. Quality & Quantity. A caution regarding rules of thumb for variance
848 inflation factors 41, 673–690.
- 849 Oliveira, G.G., Pedrollo, O.C., Castro, N.M., 2015. Simplifying artificial neural network models
850 of river basin behaviour by an automated procedure for input variable selection.
851 *Engineering Applications of Artificial Intelligence* 40, 47–61.
- 852 Paola, J.D., Schowengerdt, R.A., 1995. A review and analysis of backpropagation neural
853 networks for classification of remotely-sensed multi-spectral imagery. *International
854 Journal of remote sensing* 16, 3033–3058.
- 855 Park, S., Im, J., Jang, E., Rhee, J., 2016. Drought assessment and monitoring through blending of
856 multi-sensor indices using machine learning approaches for different climate regions.
857 *Agricultural and forest meteorology* 216, 157–169.
- 858 Parvin, F., Ali, S.A., Calka, B., Bielecka, E., Linh, N.T.T., Pham, Q.B., 2022. Urban flood
859 vulnerability assessment in a densely urbanized city using multi-factor analysis and
860 machine learning algorithms. *Theoretical and Applied Climatology* 1–21.
- 861 Paul, G.C., Saha, S., 2019. Spatial prediction of susceptibility to gully erosion in Jainti River
862 basin, Eastern India: a comparison of information value and logistic regression models.
863 *Modeling Earth Systems and Environment* 5, 689–708.
- 864 Pham, B.T., Nguyen-Thoi, T., Qi, C., Van Phong, T., Dou, J., Ho, L.S., Van Le, H., Prakash, I.,
865 2020. Coupling RBF neural network with ensemble learning techniques for landslide
866 susceptibility mapping. *Catena* 195, 104805.

- 867 Pham, Q., Pal, S., Chakraborty, R., Norouzi, A., Golshan, M., Ogunrinde, T., Janizadeh, S.,
 868 Khedher, K., Tran Anh, D., 2021. Evaluation of various boosting ensemble algorithms
 869 for predicting flood hazard susceptibility areas Evaluation of various boosting ensemble
 870 algorithms for predicting flood hazard susceptibility areas. *Geomatics, Natural Hazards
 871 and Risk* 12, 2607–2628. <https://doi.org/10.1080/19475705.2021.1968510>
- 872 Pham, Q.B., Ali, S.A., Bielecka, E., Calka, B., Orych, A., Parvin, F., Lupikasza, E., 2022. Flood
 873 vulnerability and buildings' flood exposure assessment in a densely urbanised city:
 874 comparative analysis of three scenarios using a neural network approach. *Natural
 875 Hazards* 1–39.
- 876 Poesen, J., Nachtergaele, J., Verstraeten, G., Valentin, C., 2003. Gully erosion and
 877 environmental change: importance and research needs. *Catena* 50, 91–133.
- 878 Pourghasemi, H.R., Moradi, H.R., Fatemi Aghda, S.M., Gokceoglu, C., Pradhan, B., 2014. GIS-
 879 based landslide susceptibility mapping with probabilistic likelihood ratio and spatial
 880 multi-criteria evaluation models (North of Tehran, Iran). *Arab J Geosci* 7, 1857–1878.
 881 <https://doi.org/10.1007/s12517-012-0825-x>
- 882 Pourghasemi, H.R., Sadhasivam, N., Kariminejad, N., Collins, A.L., 2020. Gully erosion spatial
 883 modelling: Role of machine learning algorithms in selection of the best controlling
 884 factors and modelling process. *Geoscience Frontiers* 11, 2207–2219.
- 885 Pradhan, B., Oh, H.-J., Buchroithner, M., 2010. Weights-of-evidence model applied to landslide
 886 susceptibility mapping in a tropical hilly area. *Geomatics, Natural Hazards and Risk* 1,
 887 199–223. <https://doi.org/10.1080/19475705.2010.498151>
- 888 Quarteroni, A., Veneziani, A., 2003. Analysis of a geometrical multiscale model based on the
 889 coupling of ODE and PDE for blood flow simulations. *Multiscale Modeling &
 890 Simulation* 1, 173–195.
- 891 Quevedo, R.P., Maciel, D.A., Uehara, T.D.T., Vojtek, M., Renno, C.D., Pradhan, B., Vojtekova,
 892 J., Pham, Q.B., 2021. Consideration of spatial heterogeneity in landslide susceptibility
 893 mapping using geographical random forest model. *Geocarto International* 1–24.
- 894 Rahmati, O., Haghizadeh, A., Pourghasemi, H.R., Noormohamadi, F., 2016. Gully erosion
 895 susceptibility mapping: the role of GIS-based bivariate statistical models and their
 896 comparison. *Natural Hazards* 82, 1231–1258.
- 897 Rahmati, O., Kalantari, Z., Ferreira, C.S., Chen, W., Soleimanpour, S.M., Kapović-Solomun, M.,
 898 Seifollahi-Aghmiuni, S., Ghajarnia, N., Kazemabady, N.K., 2022. Contribution of
 899 physical and anthropogenic factors to gully erosion initiation. *Catena* 210, 105925.
- 900 Rahmati, O., Tahmasebipour, N., Haghizadeh, A., Pourghasemi, H.R., Feizizadeh, B., 2017.
 901 Evaluating the influence of geo-environmental factors on gully erosion in a semi-arid
 902 region of Iran: An integrated framework. *Science of The Total Environment* 579, 913–
 903 927. <https://doi.org/10.1016/j.scitotenv.2016.10.176>
- 904 Roy, J., Saha, S., 2021. Integration of artificial intelligence with meta classifiers for the gully
 905 erosion susceptibility assessment in Hinglo river basin, Eastern India. *Advances in Space
 906 Research* 67, 316–333.

- 907 Roy, J., Saha, S., 2019. Landslide susceptibility mapping using knowledge driven statistical
908 models in Darjeeling District, West Bengal, India. *Geoenviron Disasters* 6, 11.
909 <https://doi.org/10.1186/s40677-019-0126-8>
- 910 Saha, S., Roy, J., Arabameri, A., Blaschke, T., Bui, D.T., 2020. Machine learning-based gully
911 erosion susceptibility mapping: A case study of eastern India. *Sensors (Switzerland)* 20.
912 <https://doi.org/10.3390/s20051313>
- 913 Saha, S., Roy, J., Pradhan, B., Hembram, T.K., 2021. Hybrid ensemble machine learning
914 approaches for landslide susceptibility mapping using different sampling ratios at East
915 Sikkim Himalayan, India. *Advances in Space Research* 68, 2819–2840.
- 916 Scherr, S.J., 2000. A downward spiral? Research evidence on the relationship between poverty
917 and natural resource degradation. *Food policy* 25, 479–498.
- 918 Shafizadeh-Moghadam, H., Tayyebi, A., Helbich, M., 2017. Transition index maps for urban
919 growth simulation: application of artificial neural networks, weight of evidence and fuzzy
920 multi-criteria evaluation. *Environmental monitoring and assessment* 189, 1–14.
- 921 Shit, P.K., Bhunia, G.S., Pourghasemi, H.R., 2020. Gully erosion susceptibility mapping based
922 on bayesian weight of evidence, in: *Gully Erosion Studies from India and Surrounding*
923 *Regions*. Springer, pp. 133–146.
- 924 Sissakian, V., Al-Ansari, N., Knutsson, S., 2013. Sand and dust storm events in Iraq. *Journal of*
925 *Natural Science* 5, 1084–1094.
- 926 Tairi, A., Elmouden, A., Bouchaou, L., Aboulouafa, M., 2021. Mapping soil erosion-prone sites
927 through GIS and remote sensing for the Tifnout Askaoun watershed, southern Morocco.
928 *Arabian Journal of Geosciences* 14, 1–22.
- 929 Tien Bui, D., Shirzadi, A., Shahabi, H., Chapi, K., Omidavr, E., Pham, B.T., Talebpour Asl, D.,
930 Khaledian, H., Pradhan, B., Panahi, M., 2019. A novel ensemble artificial intelligence
931 approach for gully erosion mapping in a semi-arid watershed (Iran). *Sensors* 19, 2444.
- 932 Turner, B.L., Menendez III, H.M., Gates, R., Tedeschi, L.O., Atzori, A.S., 2016. System
933 dynamics modeling for agricultural and natural resource management issues: Review of
934 some past cases and forecasting future roles. *Resources* 5, 40.
- 935 Vandekerckhove, L., Poesen, J., Govers, G., 2003. Medium-term gully headcut retreat rates in
936 Southeast Spain determined from aerial photographs and ground measurements.
937 *CATENA, Gully Erosion and Global Change* 50, 329–352.
938 [https://doi.org/10.1016/S0341-8162\(02\)00132-7](https://doi.org/10.1016/S0341-8162(02)00132-7)
- 939 Wang, Z., Zhang, G., Wang, C., Xing, S., 2022. Assessment of the gully erosion susceptibility
940 using three hybrid models in one small watershed on the Loess Plateau. *Soil and Tillage*
941 *Research* 223, 105481.
- 942 Wassie, S.B., 2020. Natural resource degradation tendencies in Ethiopia: a review.
943 *Environmental systems research* 9, 1–29.
- 944 Yang, A., Wang, C., Pang, G., Long, Y., Wang, L., Cruse, R.M., Yang, Q., 2021. Gully erosion
945 susceptibility mapping in highly complex terrain using machine learning models. *ISPRS*
946 *International Journal of Geo-Information* 10. <https://doi.org/10.3390/ijgi10100680>

- 947 Yin, J., Su, S., Xun, J., Tang, T., Liu, R., 2020. Data-driven approaches for modeling train
948 control models: Comparison and case studies. *ISA Transactions* 98, 349–363.
949 <https://doi.org/10.1016/j.isatra.2019.08.024>
- 950 Yuan, L., Sinshaw, T., Forshay, K.J., 2020. Review of Watershed-Scale Water Quality and
951 Nonpoint Source Pollution Models. *Geosciences* 10, 25.
952 <https://doi.org/10.3390/geosciences10010025>
- 953 Zabihi, M., Mirchooli, F., Motevalli, A., Darvishan, A.K., Pourghasemi, H.R., Zakeri, M.A.,
954 Sadighi, F., 2018. Spatial modelling of gully erosion in Mazandaran Province, northern
955 Iran. *Catena* 161, 1–13.
- 956 Zhang, S., Cheng, D., Deng, Z., Zong, M., Deng, X., 2018. A novel kNN algorithm with data-
957 driven k parameter computation. *Pattern Recognition Letters, Special Issue on Pattern*
958 *Discovery from Multi-Source Data (PDMSD)* 109, 44–54.
959 <https://doi.org/10.1016/j.patrec.2017.09.036>
- 960 Zhou, Q., Liu, X., 2004. Analysis of errors of derived slope and aspect related to DEM data
961 properties. *Computers & Geosciences* 30, 369–378.
962

Gully Erosion Inventory



Hybrid ML implementations

Weight of evidence model

$$W_i^+ = \ln \left(\frac{P\{GS|GF\}}{P\{GS|\overline{GF}\}} \right)$$

$$W_i^- = \ln \left(\frac{P\{\overline{GS}|GF\}}{P\{\overline{GS}|\overline{GF}\}} \right)$$

Geo-environmental factors

Slope Aspect Elevation

LULC Plan curvature

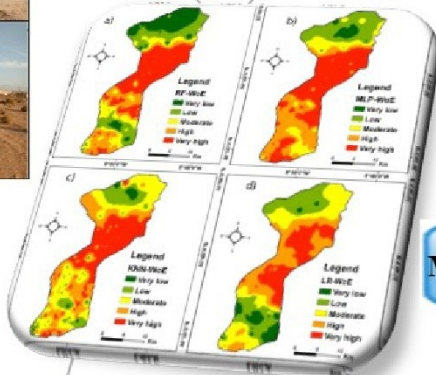
Lithology Rainfall

TWI NDVI

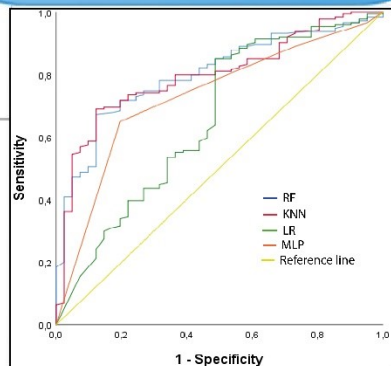
Distance to Faults

Distance to streams

Distance to Roads



Models' performance evaluation



Class 1

